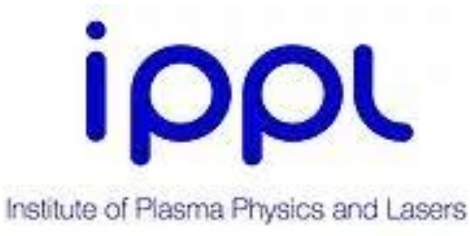

HELLENIC MEDITERRANEAN UNIVERSITY

DEPARTMENT OF ELECTRONIC ENGINEERING

& INSTITUTE OF PLASMA PHYSICS AND LASERS

MASTER THESIS

Study of High Harmonic Generation in a semi-infinite gas cell, generated by ultrashort femtosecond laser pulses.

Frantzeskakis Nikolaos

Advisory Committee

Prof. Nektarios A. Papadogiannis

Assoc. Prof. Efthimios Bakarezos

Asst. Prof. Emmanuel Benis

Examination Committee

Prof. Nektarios A. Papadogiannis

Prof. Michael Tatarakis

Asst. Prof. Emmanuel Benis

ACKNOWLEDGEMENTS

First of all, I would like to thank my supervisor, Professor Nektarios Papadogiannis (Hellenic Mediterranean University), for his substantial guidance in my effort to carry out this master thesis. His long year occupation in the domain of High Harmonics and his knowledge according to experimental procedure, were fundamental for me, in order to understand High Harmonic Generation and their spectra analysis.
Furthermore, I would like to thank Professors M.Tatarakis (Hellenic Mediterranean University) and Em.Benis (University of Ioannina) who comprised with my supervisor the examination committee of my thesis.
In addition, I thank Professor Efthimios Bakarezos (Hellenic Mediterranean University) as a member of the advisory committee. Finally, I would like to refer the name of Stelios Petrakis, who helped me essentially to carry out the necessary experiments, to obtain data for the writing of this master thesis.

Frantzeskakis Nikolaos,
Rethymno 2021

Nikolaos Frantzeskakis, MSc-Hellenic Mediterranean University

ABSTRACT

The topic that is investigated in this Master Thesis is related with the "***Study of High Harmonic Generation in Semi-Infinite Gas cell by ultrashort laser pulses***". The time duration of these pulses is about of few femtoseconds.

In the first chapter, the theoretical background of High Harmonic Generation (HHG) is presented. More specifically there is a description of a semi-classical model, in order to explain how higher harmonics occur, called the "*Three Step Model*''. Afterwards, the factors that affect the phase matching between the fundamental laser pulse and each harmonic (q^{th} order) pulse are adduced (*Phase Matching Theory*). In addition, the experimental concept of Semi-Infinite Gas Cell is presented and the parameters that can play a major role in the generation of higher harmonics, such as the aperture of the fundamental beam, its focus conditions and the pressure of the gas in the cell.

In the second chapter, the essential experimental equipment and the procedure followed, in order to generate and detect higher order harmonics, are analytically described.

In the third chapter, the diagrams of Vacuum Ultraviolet radiation amplitude versus wavelength for three different gases media: Argon (Ar), Neon (Ne) and Nitrogen (N) are presented. In the first experiments the pressure of the gases media and the intensity of the fundamental laser beam are kept constant in order to study the effect of gas nature to the HHG. Later, for the case of Argon, we investigate the behavior of the spectrum of the generated harmonics for varying the pressure of the gas in the cell and the focus position of the fundamental beam in respect to the semi-level between gas and vacuum.

In the last chapter of this thesis, the conclusions are presented after the analysis of the detected HHG spectra.

The experiments for the thesis were carried out in spring 2020, in the ***Institute of Plasma Physics and Lasers*** (IPPL) of Hellenic Mediterranean University, in Tria Monastiria Rethymno.

CONTENTS

CHAPTER 1:HIGH HARMONIC GENERATION

1.1 INTRODUCTION

High Harmonic Generation occurs when a high intensity light pulse interacts with a nonlinear medium (atomic/ molecular gas or solid). For laser pulse ~ 10^{13}-10^{14} W/cm^2 , atoms become partly ionized and the outer electrons are driven by the linearly polarized Electric Field of the laser, in an oscillating motion around their parent nuclei. Some of them recombine with parent nucleus, emitting secondary radiation. Due to the time characteristics of this phenomenon and the centrosymmetry in the case of the atoms, secondary radiation is emitted in frequencies which are odd multiples of fundamental laser frequency. High Harmonics are generated by focusing ultra short laser pulses, with duration a few *femtoseconds* (1*fs*=10^{-15}s), and with intensity which can partly ionize the atoms of active medium.

With our available means, we have managed to generate harmonics in the regime of *VUV ή XUV* [1]up to Soft X-rays see for example in XUV[1] and soft X ray part of radiation spectrum [2]. Generation of ultra short pulses in these spectrum regimes has offered various applications in sciences like Physics, Chemistry, Biology and Biochemistry.

One of those applications, is the formation of attosecond pulses (1as= 10^{-18}s) [3]. These emitted pulses can have the shape of a ‘‘train of pulses’’ or an isolated pulse and occur when the generated harmonics come to phase matching (*phase locked harmonics)*.Furthermore applications can be observed in the domain of *time resolved ultrafast dynamics* [4,5].

1.2 THEORETICAL BACKGROUND

1.2.1 NON LINEAR OPTICS

Non-Linear Optics is a physics domain, which was developed after laser invention (1960) and especially after pulsed lasers invention. In fact, it is the correction of Linear Optics. According to Linear Optics the polarization of a material is a linear function of the applied Electric Field.

$$P = \varepsilon_0 \chi E \tag{1.1}$$

x is linear susceptibility of material and ε_0 the vacuum dielectric constant **.**

However, when the laser Electric Field becomes comparable to atomic Coulomb Potential, non-linear terms of the induced polarization are important. Applying Taylor expansion polarization can be written:

$$P = \varepsilon_0 \chi^{(1)} E + \varepsilon_0 \chi^{(1)} E^2 + \varepsilon_0 \chi^{(3)} E^3 + \cdots \tag{1.2}$$

The first order term refers to linear susceptibility, the second one to the first order nonlinear susceptibility etc. HHG is a nonlinear procedure which takes place when Electric Field is efficiently strong. The necessary intensity of the fundamental beam must be at least $10^{13} W/cm^2$. Such intensities can be achieved by focusing a femtosecond laser beam in a target of noble gas. For higher intensities, the contribution of nonlinear terms of Eq.1.2 becomes significant. Finally, there is an upper limit of laser intensity for HHG. For intensities higher than $\sim 10^{16} \frac{W}{cm^2}$, the increased magnetic field prohibits the recombination of the electron with the nucleus and consequently HHG. In addition self focusing of the beam and plasma generation can act as limiting factors for HHG, as an important part of outer electrons are completely ionized.

The refractive index of a non-linear medium can be extracted by the equation:

$$n = n_0 + n_2 I \tag{1.3}$$

n_0 is the *weak field refractive index* and n_2 is the non-linear term which shows how refractive index changes with the intensity of laser beam. The non-linear refractive index is given by the equation:

$$n_2 = \frac{3}{2{n_0}^2 \varepsilon_0} \chi^{(3)} \tag{1.4}$$

1.2.2 THREE STEP MODEL

Three Step Model is a model that reasonably explains all the experimental results in HHG and provides a clear understanding of High Harmonic Generation procedure. It was developed by P.B.Corkum [6]. In fact, this semi classical model is valid only in limit of Quantum Tunneling ($h\omega_0 << I_p << U_p$). I_p is the ionization potential of the atom and U_p is called *pondermotive energy*, corresponding to the mean kinetic energy of a free electron which oscillates by laser field with frequency ω_0 and intensity I.

In the Three Step Model, High Harmonic Generation is explained in three steps.

1. An atom that is irradiated by a strong laser field can partly release during a time interval of t_i, an outer electron. As a result a parent ion and a partly free electron, without kinetic energy, occur.

2. The electron is accelerated by laser electric field. When the electric field changes its sign, it can (with a possibility) drive the electron back, close to the nucleus.

3. When the electron comes close to the area of nucleus, then the ion and the electron may recombine and the total extra energy (electron kinetic energy Ec, plus binding energy I_p) is released as the energy that a photon emits.

$$\hbar\omega = E_c + I_p \tag{1.5}$$

The three steps mentioned above are shown in the figure below

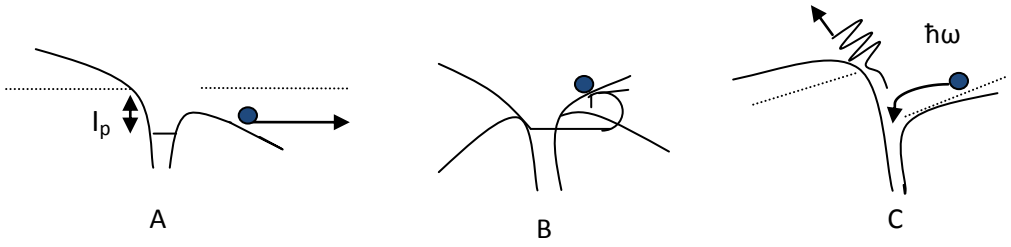

Fig.1.1 Three Step Model for High Harmonic Generation (HHG).
A. Ionization through Quantum Tunneling, B.Acceleration by laser electric field, C.Recombination and emission of energy.

In the figure below a typical spectrum HHG for atomic gases is presented.

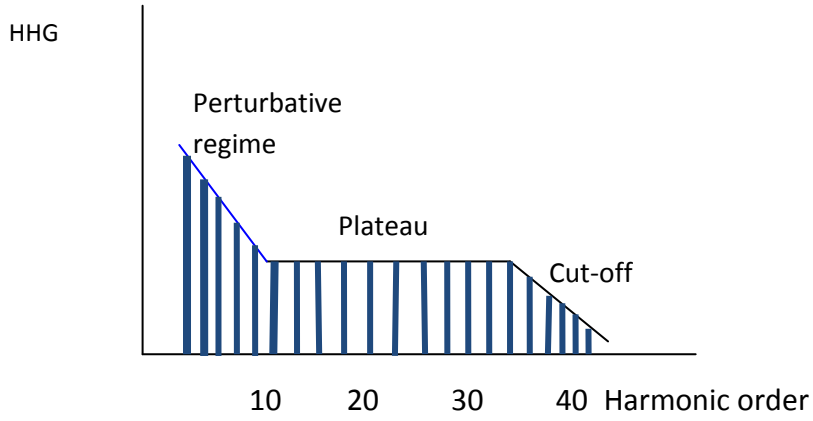

Fig.1.2 A typical HHG spectrum for atomic gases [7]

Firstly, we observe that for low order harmonics, intensity reduces as the order increases. Afterwards, it takes a constant value (plateau) and finally for high harmonic orders, intensity reduces up to cut-off frequency. In the spectrum we observe only odd harmonics (ω_n= (2n+1) ω_0) where ω_0 is fundamental laser frequency, due to the fact that the material in which HHG occurs, is centro-symmetric. During half cycle of laser period, after the ionization, the electron returns to the parent ion to recombine and the electric field changes sign. Consequently, harmonics are generated twice during a laser cycle. The time interval in which harmonics are emitted corresponds to the half of laser period. Using Fourier *transform* this separation of harmonics, in time interval equal to the half of period in *time domain*, results in peaks separated by $2\omega_0$ in *frequency domain*. The even harmonics (ω_n=2*n* ω_0) interfere constructively, as their spectral components have the same amplitude but inverse phase, contrary to the odd harmonics, which interfere constructively and can be observed in emission spectrum.

1.2.2.A) ATOMIC IONIZATION THROUGH QUANTUM TUNNELING

In the Quantum Tunneling regime, the expression $h\omega_0 << I_p$ states that the absorption of a lot of photons is necessary for atomic ionization. As a result, an accurate description of ionization mechanisms requires a lot of simulations and non perturbative methods. However, in this domain the photonic character of laser field can be partially neglected and semi-classical simulations have been successfully developed to simulate the strong ionizaton of field-atom through Quantum Tunneling.

According to these models, an atom is described as an ionic nucleus and an electron. The ionic nucleus creates a Coulomb potential in which the electron evolves. The strong laser field is simply considered as an electric field $E(t) = E_0(t) \cos(\omega_0 t)$ which oscillates slowly. When an atom is irradiated by a strong laser field, the total potential is the sum of ionic nucleus potential and the electric interaction potential. When this field is very strong, the electron has a possibility to escape from ionic nucleus through quantum tunneling.

An important parameter is *Keldysh parameter* which is defined as:

$$\gamma = \sqrt{\frac{I_p}{2U_p}} \tag{1.6}$$

Quantum tunneling is observed for *γ*<1. For *γ*>1 *multiphoton ionization*, is observed while for γ<<1 *above threshold ionization* takes place [8].

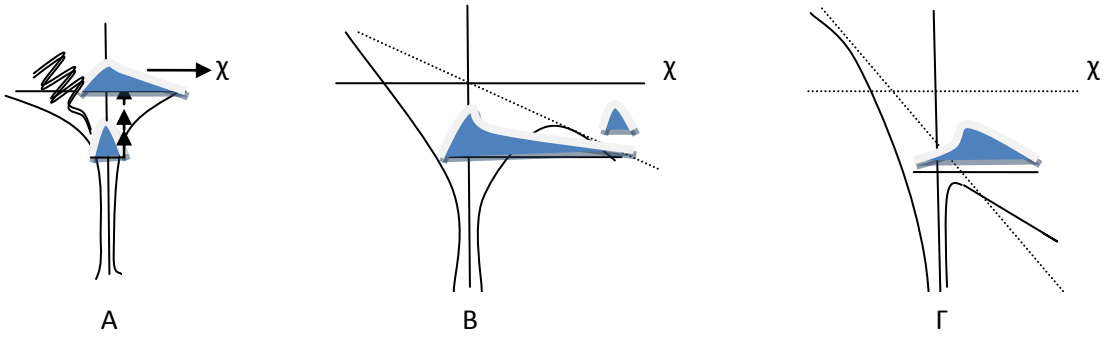

Fig. 1.3 A) multiphoton ionization, B) Quantum tunneling, C) above threshold ionization

The possibility an electron to escape through Quantum Tunneling from a potential well is known and depends on the initial energy level I_p for an atom at ground state and the depth of the barrier. A general formula for the description of atomic ionization was developed by *Ammossov, Delone and Krainov* (*ADK Theory*) [9]. Rate ionization in ADK theory is given by:

$$W_{ADK}{}^{lin} = |C_{n^*l^*}|^2 G_{lm} I_p \left(\frac{2F_0}{F}\right)^{2n^*-|m|-1} \exp\left(-\frac{2F_0}{3F}\right) \tag{1.7}$$

$$W_{ADK}{}^{cir} = \sqrt{\frac{3FZ^3}{\pi n^{*3}}}\left(\frac{4Z^3 e}{Fn^{*4}}\right)^{2n^*-1} \exp\left(-\frac{2Z^3}{3Fn^{*3}}\right) \tag{1.8}$$

Where *Z* is *charge state*, $n^* = \frac{Z}{\sqrt{2I_p}}$ is *effective principal quantum number*), $F_0 = (2I_p)^{\frac{3}{2}}$, *m* is *magnetic quantum number* and *F* is *electric E-field strength*. Constants G_{lm}, $|C_{n^*l^*}|^2$ are given by the formulas below:

$$G_{lm} = \frac{(2l+1)(l+|m|)!}{2^{|m|}|m|!\,(l-|m|)!} \tag{1.9}$$

$$|C_{n^*l^*}|^2 = \frac{2^{2n^*}}{(n^*\Gamma[n^*+l^*+1]\Gamma[n^*-l^*])} \tag{1.10}$$

Where l^* is effective *optical quantum number* and Γ is *gamma function.*

Then the ionization possibility can be derived from:

$$p = 1 - e^{-\int_{-\infty}^{+\infty} W_{ADK}(t)dt} \quad (1.11)$$

1.2.2.B) ELECTRON ACCELERATION BY LASER ELECTRIC FIELD

As it was mentioned before the first step of Three Step Model is the escape of the electron by nucleus potential through Quantum Tunneling. Afterwards the electro is accelerated by laser electric field.

The classical motion of an electron in an AC Electric field is given by Newton's 2nd Law:

$$m\frac{\partial^2 \mathrm{r}}{\partial \mathrm{t}^2} = -eEcos\,(\omega_0 \mathrm{t} + \varphi) \quad (1.12)$$

Where φ is initial ionization phase and ω_0 the frequency of the oscillation of AC electric field.

Firstly, the free electron starts to move away from the ion. However, the laser field changes sign after a quarter of laser period, resulting in electron deceleration, which afterwards is immobilized away from the ion and then accelerates towards it. During this motion the electron gains extra kinetic energy. When the electron comes back, it is possible to recombine with the ion and emit radiation.

The extra kinetic energy is transferred into the emitted radiation. For a linearly polarized field, along *x axis,* we have:

$$m\frac{\partial^2 \chi}{\partial \mathrm{t}^2} = -eEcos\,(\omega_0 \mathrm{t} + \varphi) \quad (1.13)$$

By Eq.1.13 we can calculate electron velocity:

$$u(t) = -\frac{e}{m_{e\omega_0}} E(\sin(\omega_0 t + \varphi) - sin\varphi) \quad (1.14)$$

By integrating Eq.1.14 we derive an expression for the position $\chi(t)$ of the electron:

$$\chi(t) = \frac{-e}{m_e \omega^2} E[cos(\omega_0 t + \varphi) - cos(\varphi)] + sin(\varphi)t \quad (1.15)$$

In Fig.1.4 electron trajectories are plotted for different values of phase ionization. We observe that, there are electrons which do not return at x=0 to recombine with the nucleus. Radiation emission happens for a small part of phases.

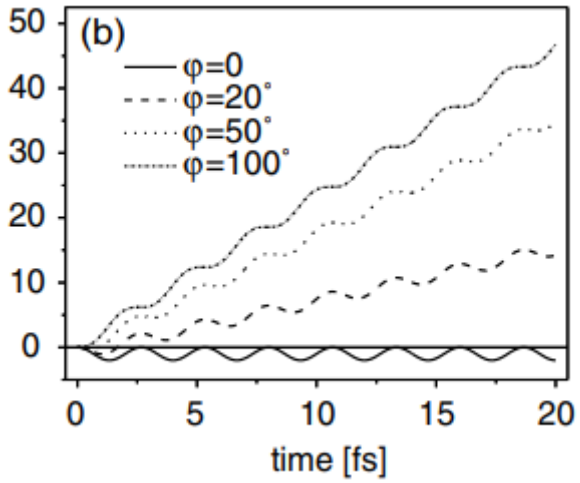

Fig.1.4 Electron trajectories for different values of phase ionization taken by Ref. [10].

For zero initial kinetic energy, the mean kinetic energy of an electron is:

$$U_p = \frac{q^2 E^2}{4m{\omega_0}^2} \tag{1.16}$$

The term *Up* is called *ponderomotive energy*. We can consider it as the mean kinetic energy of an electron, which moves in an *AC Electric Field*:

$$U_p(\text{eV}) = 9.33 \times 10^{-14}\, I(W) * \lambda^2\,(cm^{-2}) \tag{1.17}$$

HHG takes place at the limit of Quantum Tunneling ($h\omega_0 << I_p$)and is related to ponderomotive energy. The *cut-off* frequency is given by the equation:

$$h\,\omega_c = I_p + 3.17U_p \tag{1.18}$$

Eq.1.16 is called the *cut-off law***.**

The equation above gives the maximum energy of an emitted photon, which occurs during the recombination of the electron with the nucleus. By replacing $\omega_c = q_{max}\,\omega_0$ we can calculate that the highest harmonic order is:

$$q_{max} = \frac{I_p + 3.17U_p}{h\omega_0} \tag{1.19}$$

The highest harmonic order observed, depends on the ponderomotive energy and ionization potential of the used gas.

The first condition is achieved by increasing the wavelength or the intensity of laser beam. The second one is achieved by selecting atoms, such as noble gases, which have relatively high ionization potential.

1.2.2. C) ELECTRON TRAJECTORIES AND RECOMBINATION

In the previous sections, we saw that an electron escapes initially from the nucleus potential, through Quantum Tunneling, and afterwards is accelerated by laser electric field, which interacts with the atoms of the active medium.

In the beginning the electrons accelerate far away from the nucleus because of the effect of laser AC field. Afterwards, the sign of electric field changes and the electrons are forced to move towards the nucleus. Then it is possible to recombine with the nucleus and emit light.

An electron which recombines with the nucleus of the atom, that it comes from, obtains energy equal to the sum of ionization potential I_p and its kinetic energy K.

The maximum kinetic energy for a linearly polarized field is:

$$K_{max} = 3.17U_p \qquad (1.20)$$

The maximum energy of a photon is given by eq.1.16

There are two different trajectories that an electron can follow, which correspond to the same energy in the harmonic spectrum. These trajectories have different *travel time* (time interval between the ionization of an atom and the recombination of the electron with the nucleus and ionization time). The t_{travel} (*travel time*) equal to 0.65T, (T is the period of E-Field oscillation), corresponds to the maximum recombination energy. For t_{travel} > 0.65T *long trajectories* are observed, while for t_{travel}<0.65T *short trajectories* are observed.

t_{travel} > 0.65T → *long trajectories*

t_{travel} < 0.65T→ *short trajectories*

The different harmonic orders occur because of different *emission times* t_e and the different trajectories the electron follow in order to recombine with the nucleus.

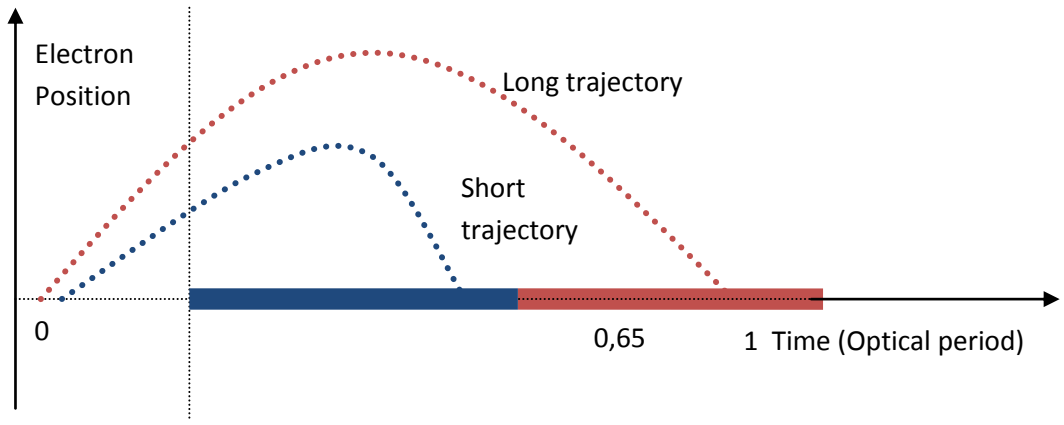

Fig.1.5 Qualitative plot of short and long trajectories.

1.3 PHASE-MATCHING THEORY

To enhance harmonic emission, the wave front of fundamental frequency must be in phase matching with the wave front of the harmonics. When this condition is fulfilled, enhancement of generated harmonics is observed. To describe phase matching, we induce *coherence length* (L_{coh}). This quantity is the distance in which constructive interference takes place.

$$L_{coh}=\frac{\pi}{\Delta\kappa_q} \tag{1.21}$$

$\Delta\kappa_q$ is the phase mismatch vector between fundamental frequency and the harmonic frequency of qth order. When perfect phase matching is achieved:

$$\Delta\kappa_q= qk(\omega) - k(q\omega) = 0 \tag{1.22}$$

According to [11] the intensity of q^{th} harmonic at the end of active medium, without taking into consideration the absorption is given by the formula:

$$I_q \propto L^2 \frac{(sin\left(\frac{L\Delta kq}{2}\right))^2}{\left(\frac{L\Delta kq}{2}\right)^2} \tag{1.23}$$

Where L is the medium length

Generally the $\Delta\kappa_q$ mismatch vector is the sum of four terms [12].

$$\Delta\kappa_q=\Delta\kappa_{q,geo} + \Delta\kappa_{q,plasma} + \Delta\kappa_{q,neutral} - \Delta\kappa_{q,dip} \tag{1.24}$$

We analyze each one of these four terms below.

In the picture below we show the dependence of intensity by the medium of active length. Specifically, when phase matching is achieved the intensity is proportional to the square of the length of active medium.

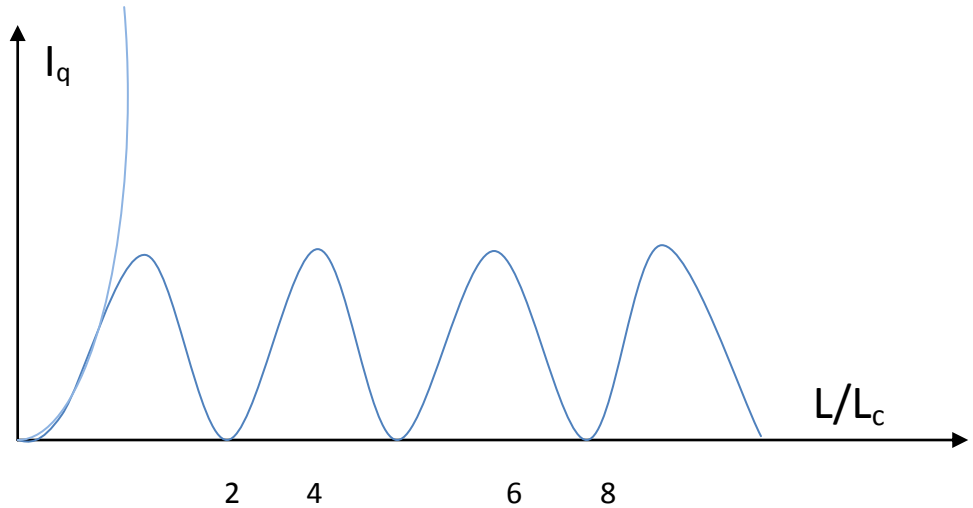

Fig.1.6 Intensity of q^{tn} order harmonic as a function of medium length

The geometrical term $\Delta\kappa_{q,geo}$

To reach sufficiently high values of intensity necessary for efficient HHG we have to focus the laser beam. When the wave front comes through a focus it experiences a phase shift, leading to divergence between laser wave front and the wave front of a plane wave. For a Gaussian beam a geometrical time phase (*Gouy Phase*) is appeared and is given by the equation:

$$\varphi_{Gouy}(z) = tan^{-1}(\frac{z}{z_R}) \quad (1.25)$$

Where z_R is called *Rayleigh length*:

$$\kappa_{geo}(z) = \frac{d\varphi_{Gouy\ (z)}}{dz} = \frac{dtan^{-1}(\frac{z}{z_R})}{dz} \quad (1.26)$$

The geometric contribution in the total mismatch vector is:

$$\Delta\kappa_{q,geo} = q\kappa_{geo}(\omega) - \kappa_{geo}(q\omega) \quad (1.27)$$

We can assume that the fundamental beam has the same geometric phase with the harmonics, for at least a length equal to z_R. $\kappa_{geo}(\omega) \approx \kappa_{geo}(q\omega)$

The final formula for the geometric term phase matching is given as:

$$\Delta\kappa_{q,geo} = \frac{q-1}{z_R\ [1 + \left(\frac{z}{z_R}\right)^2]} \quad (1.28)$$

For distances very close to the focus ($z \simeq 0$): $\Delta\kappa_{q,geo} = (q-1)/z_R$

The contribution of the geometric term is positive ($\Delta\kappa_{q,geo} > 0$).
The related coherence length (for $z \simeq 0$) is given as:

$$L_{c,geo} = \frac{\pi z_R}{q} \quad (1.29)$$

Another way to control the contribution of geometric term in the total mismatch vector is to remove the focus position in relation to the medium.

$\Delta\kappa_{q,geo}$ term – Dispersion due to plasma generation

The second term in phase mismatch vector is due to dispersion because of plasma generation. When a high intensity laser pulse interacts with a medium, a partial ionization of atoms and electron emission are observed. Most of the electrons do not recombine with the nuclei. The generated plasma consists of free electrons and positively charged nuclei.

The plasma contribution in total mismatch vector is due to exclusively in electrons because of their small mass in comparison with the mass of nucleus.

The electrons absorb the incident light and carry out collective oscillations.

These oscillations result in the change of refraction index. The plasma frequency of electrons is given by:

$$\omega_p = \sqrt{\frac{Ne^2}{m\varepsilon_0}} \tag{1.30}$$

Where N_e is electron number per volume unit, $\boldsymbol{\varepsilon_0}$ is dielectric constant of vacuum, e is electron charge and m its mass. The induced plasma refraction index is given by:

$$n_p = \sqrt{1 - \frac{{\omega_p}^2}{\omega^2}} = \sqrt{1 - \frac{N_e}{N_c}} \tag{1.31}$$

Where ω, ω_p are laser and plasma frequency, N_c is critical density of electrons:

$$N_c = \frac{m\omega^2\varepsilon_0}{e^2} \tag{1.32}$$

We know that density of free electrons is orders of magnitude lower than the critical density. By using Taylor expansion of Eq.1.31 and keeping the first two terms constant (the most important of the expansion) we end up with equation:

$$n_p = 1 - \frac{1}{2}\left(\frac{\omega_p}{\omega}\right)^2 \tag{1.33}$$

From the above equation we conclude that refraction index because of plasma dispersion is lower than unity. Finally, we conclude that the contribution of plasma in mismatch vector is given by**:**

$$k_p(\omega) = \left(n_p - 1\right)\frac{\omega}{c} \approx -\frac{{\omega_P}^2}{2c\omega}(1.32) \tag{1.34}$$

The mismatch vector because of plasma can be calculated as:

$$\Delta\kappa_q \text{ , plasma} = qk_p(\omega) - k_p(q\omega) = \frac{\omega_p(1 - q^{2})}{2qc\omega} \tag{1.35}$$

Note that the contribution in mismatch vector because of plasma is negative.

$\Delta\kappa_{q,neutral}$ term -Dispersion due to neutral atoms

Another contribution in phase matching is dispersion because of neutral atoms. This dispersion is owed to the dependence of wavelength by refraction index. In particular the fundamental laser frequency and the generated harmonics have different refraction indexes. We can write that:

$$k_{neut(\omega)} = [n(\omega)-]\frac{\omega}{c} \tag{1.36}$$

As a result:

$$\Delta\kappa_q\,, neutral = qk_{0,neut} - k_{p,neut} = q\frac{\omega_0}{c}(n_{laser}-1) - q\frac{\omega_0}{c}(n_{harmonic}-1)$$

$$\Delta\kappa_q\,, neutral = \frac{2\pi q}{\lambda_0}(n_{laser} - n_{harmonic}) \tag{1.37}$$

By taking under consideration the dependece of pressure [13] we have:

$$\Delta\kappa_q\,, neutral = \frac{2\pi q}{\lambda_0}\frac{p}{p_0}\delta n(1-\eta) \tag{1.38}$$

Where p, p_0 are the pressure and the medium pressure in *STP* conditions correspondingly.The term δn is refraction index difference and η is the rate of atomic ionization. This equation is valid for low ionization of the medium.

When the refraction index difference is negative $\delta n<0$ then the contribution of the term $\Delta\kappa_{q,neutral}$ is negative. On the other hand when $\delta n>0$ the term $\Delta\kappa_{q,neutral}$ contributes positively in the mismatch vector.

Atomic dipole phase mismatch

The Atomic dipole phase mismatch vector is given by the equation [12] :

$$\Delta\kappa_{q,dip}=\nabla\varphi_{q,dip} \tag{1.39}$$

Where $\varphi_{q,dip}$ is the atomic dipole phase mismatch and comes from the trajectory that an electron follows for HHG. At a first approximation we consider that the atomic dipole phase is proportional to the intensity of the laser :

$$\frac{d\varphi_{dip,long}}{dI} = a \tag{1.40}$$

If we consider that the beam is gaussian:

$$\frac{\partial\varphi_{q,dip}}{\partial z} = -a\frac{\partial I}{\partial z} = \frac{8z}{b^2}\frac{1}{(1+(\frac{2z}{b})^2)^2}aI_0 \tag{1.41}$$

B is the *confocal parameter*

I_0 is the peak intensity of the gaussian beam

1.4 INTENSITY DEPENDENCE BY THE PRESSURE

When we manage to achieve phase matching between the fundamental frequency and a harmonic of order q ($\Delta\kappa_q=0$), the total emitted Electric Field E of secondary harmonic radiation has to icrease with the number of the atoms which emit(E_{HHG}~N).This number is proportional to the pressure of the atoms of the active medium.For a noble gas, we know from Ideal Gas Law that p~N. Furthermore the photon number emitted in a specific direction,or the intensity of a harmonic of order q,is proportional to the square of the Electric Field E (I_q~E^2). From the above we conclude that I_q~p^2 when perfect phase matching is achieved.

When perfect phase matching is not achieved the dependence by the pressure is given the equation below [14]:

$$I_q(P)=\frac{{\omega_q}^2}{n_q(P)(n_0(P))^q c^4 {\varepsilon_0}^2}\left|x^{(3)}(P)\right|^2 {I_1}^q \frac{sin^2\left(\frac{L_q\Delta k_q(P)}{2}\right)}{\left(\frac{L_q\Delta k_q(P)}{2}\right)^2} \qquad (1.42)$$

Where $n_0(P)$, $n_q(P)$ are the refractive indexes for the fundamental frequency and the frequency of the harmonic correspondingly.

ω_q is the frequency of qth harmonic and L_q is its coherence length

$\chi^{(3)}(P)$ is the third order nonlinear susceptibility and I_1 is the intensity of thε foundamental laser beam.

From the Eq.1.42 we conclude that the intensity of a harmonic of order q presents oscillations due to the term $sin^2[L_q\,\Delta k_q\,(P)/2]$

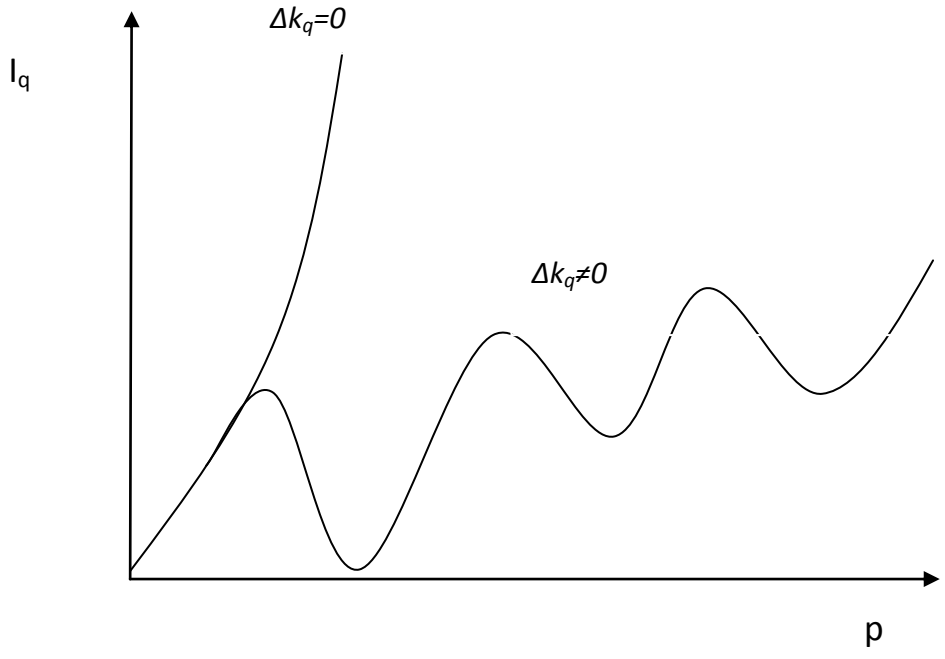

Fig.1.7 Qualitative plot of the intensity of a harmonic of order q as a function of the pressure of the gas.

1.5 *QUASI PHASE MATCHING -QPM-* IN HHG

When we cannot achieve perfect phase matching, an alternative approximation can be implemented called *Quasi Phase Matching*. By using this technique, we don't try to achieve perfect phase matching ($\Delta\kappa_q$=0).We omit the emission of harmonics only in the areas where destructive interference occurs, resulting in the increase of harmonic intensity. Through *QPM,* the mismatch vector between the fundamental frequency and the frequency of a harmonic is corrected periodically, inducing a periodicity which corresponds to the double of coherence length of the non linearity of the medium.

There are several different ways in order to achieve QPM. More specifically, we can achieve it by modulating the laser electric field (driving laser field) or the electric field of the generated harmonics.

There are various techniques we can achieve quasi phase matching e.g. by altering the *driving laser* intensity with periodically modified waveguides diameters[15] or with multi-rhythm vibration in the laser cavity [16] and using *counter propagating pulses*[17].

Alternatively, the atomic density of the medium in which harmonics are generated, can be modified by using multiple *gas jets* [18], [19], or electric discharge of the cavity [20].

1.6 SEMI-INFINITE GAS CELL

The Semi-Infinite Gas Cell- SIGC- is an experimental layout, which is used for the generation of High Harmonics. The geometry of *SIGC* permits the generation of harmonics in the XUV part of the radiation spectrum[1].

This specific layout consists of a chamber full of gas, usually a noble gas(Argon,Neon,Helium,Xenon).The fundamental laser beam(duration of a few fs) enters the cell through an entrance window. In the main chamber of the cell, the noble gas is located. The gas comes into the cell through a needle valve**.** At the end of the cell there is a pinhole from which the generated harmonics and the fundamental beam emerge. After their generation the harmonics and the fundamental beam propagate in the empty space of the cell. A schematic layout of the cell is presented in th figure below.

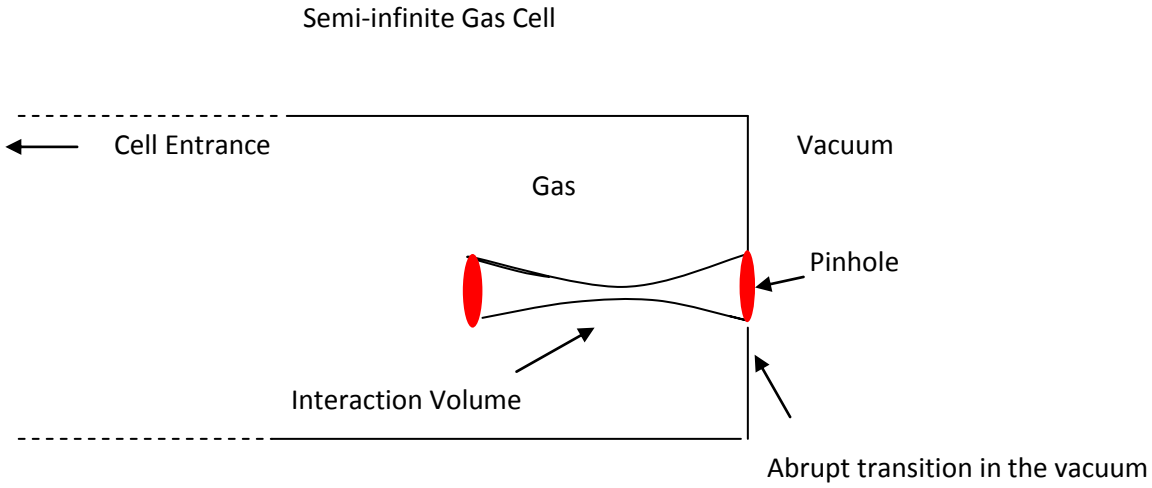

Fig.1.8 Schematic layout of Semi-infinite Gas Cell

The laser beam, before entering the cell, comes through a converging lens in order to focus into the cell and ineract with the atoms of the gas. In addition, before the beam comes through the lens, its outer diameter is modified by an aperture.It grows by opening the aperure and decreases when the aperure closes. As a result the energy of the laser beam and the dimension of focusing vary correspondingly. The experimental set up of the Semi-infinite Cell uses in this thesis, will be analyzed in detail in the chapter of experimental set up.

Various factors affect the spectum of the harmonics generated in Semi-infinite Cell. The most important are: i)the diameter of the beam, ii) the focus position of the beam into the cell, iii) the pressure of the gas.

The dependence of the harmonic spectrum by the factors above has been studied and examined in experimental point of view in this thesis. Underneath, experimental results related to the effect of those parameters, in the harmonic spectrum, are presented.

i)Dependence by the diameter of fundamental beam

It has experimentally been observed that the intensity of harmonics increases when the diameter of the apperture, from which the fundamental beam comes through,decreases up to a point, enen though the energy of fundamental beam decreases. Specifically, it has been observed an increase of the harmonic intensity for the gas Argon (Ar) by a factor 10 when the diameter of the iris- aperture decreases up to a point. All the other conditions (gas pressure, focus position, cell length, pulse energy) remain constant when the diameter of the iris changes value. In addition it is known that the intensity of each harmonic (for Xe,Ar,Ne) separately is a function of the diameter of the iris and reaches its maximum value for a specific value of diameter[21]. Such a study, we have carried out in this thesis. More specifically we observed that, by keeping the diameter of iris constant at a value, we receive the maximum intensity of generated harmonics.

ii)Dependence by the focus position of the laser beam

The geometry (e.g. focus position z_f relatively to the pinhole,volume of focusing) in which the beam of specific diameter focuses inside the cell, is an important factor which affects the harmonic generation in a Semi-infinite Gas Cell. More analytically, harmonics of different order are efficiently generated, if the focus position is out of the cell, in the vacuum chamber ($z_f>0$), inside the cell ($z_f<0$),or at the pinhole ($z_f \approx 0$).

In experiments which were carried out for harmonic generation for noble gases Helium(He) and Xenon(Xe), it was observed that harmonics of higher order are generated when we have focusing fully inside the cell ($z_f<0$), while harmonics of lower order are generated when the focus position is out of the cell ($z_f>0$). Furthermore, the intensity of each harmonic varies while the focus position changes according to Ref.[21].

iii) Dependence by the gas pressure

Another factor, which affects the spectrum of emitted harmonics in a semi- infinite gas cell, is the pressure of the gas. The variation in the spectrum of harmonics is perceived if the gas pressure changes and other conditions of the experiment such as focus position of the beam, its diameter and pulse energy remain constant.

For low pressures when conditions for perfect phase matching are fulfilled and there is not absorption of harmonics, the dependence of the intensity of harmonics as a function of the pressure follows the law $I_q \sim p^2$. For higher pressures, it has been experimentally observed the phenomenon of Saturation for harmonics of lower orders [21].

CHAPTER 2. EXPERIMENTAL EQUIPMENT/PROCEDURE FOR HIGH HARMONIC GENERATION

2.1INTRODUCTION

In this chapter of the master thesis there is description of th experimental procedure we follow for High Harmonic Generation for noble gases inside a semi-infinite cell and the equipment which is necessary for harmonic generation and record of its spectrum.

Firstly, there is a description of the system of Ti-Sa laser (Titanium-Saphire) we use and the procedure we follow to amplify the laser pulse, through *Chirp Pulse Amplification* (*CPA*) technique, before the beam enters the Semi-infinite Cell. Afterwards there is reference to the optics which drive the beam up to its entrance into the chamber of harmonic generation. Later we put emphasis on the techniques we use for the creation of the necessary vacuum. In addition there is a description of the function of harmonic grating, of the *Multichannel Plate detector* (MCP) and of the oscilloscope for the record of the MCP signal.

2.2 DESCRIPTION OF PULSED LASER TI-SA –*PULSAR*

The pulsed laser Ti-Sa (*Titanium –Sapphire*), which is used for harmonic generation is a femtosecond laser which provides energy higher than 1.0 J, with repetition rate 10Hz. The duration of the pulse is about 25 fs at FWHM. As a result the *peak power* can be higher than 45 TW. The function of the laser is based on the *Chirp Pulse Amplification* (*CPA*) technique. Particularly the system amplifies the pulses by a Ti:Sapphire Oscillator and consists of a *booster*, a device which stretches the pulse (*stretcher*), a *regenerative amplifier* and multi-pass amplifiers with corresponding *pump laser*s and an *air compressor*. Only a fraction of this laser beam is used for the experiments presented in this thesis. This is the probe beam with has a maximunt energy per pulse of about 10 mJ and a pulse duration of 25 fs.

Characterization of time duration of the laser pulse.

The time duration of the laser pulse is an important parameter because it affects the intensity of the laser beam. The measurement of the time duration of laser pulse took place with the device “Bonsaï” of the company *Amplitude Technologies*.

Fig.2.1 Counting device of the company Amplitude Technologies, we use for the measurement of time duration of laser pulse.

This device uses the technique *intensity autocorrelation*. For the measurement we take a small part of the beam through a beam splitter and we drive it in the counting device. After the necessary alignment there is collection and processing of data through a computer.

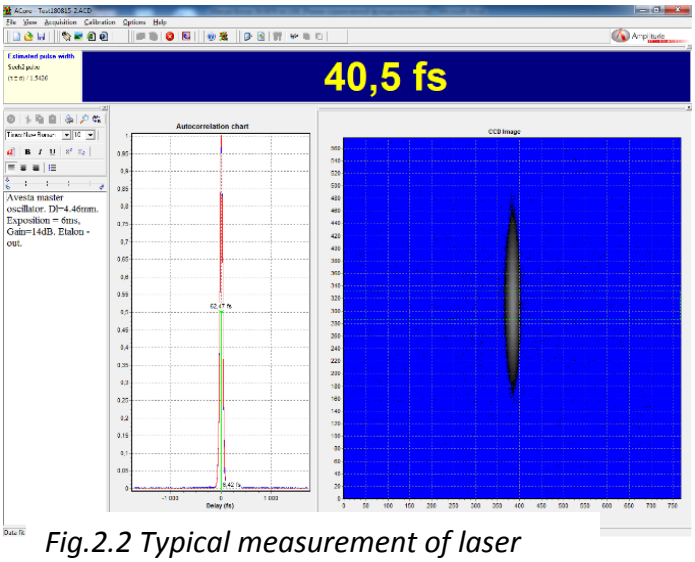

Fig.2.2 Typical measurement of laser pulse duration with the device Bonsai.

2.2.A *CHIRP PULSE AMPLIFICATION TECHNIQUE(CPA)*

The laser pulse (time duration of a couple fs) we use for our experiments is amplified through a technique called Chirp Pulse Amplification (CPA).

CPA technique is a method of amplification of laser pulses with intensities up to petawatt ($1PW=10^{15}$ W). The laser pulse is stretched in time (and space) and later is amplified and compressed in its initial time duration. The stretching and compression of the pulse requires the use of components which secure that different colours of the pulse travel in different distances.

Before the introduction of this technique the intensity of the pulse could not exceed a value, because a pulse in GW/cm^2 caused severe damage in the active medium due to nonlinear procedures, such as *self focusing*. To keep the intensity of a pulse under the limit of nonlinear phenomena, the laser system parts had to be large and expensive and their maximum intensity was limited in the area of GW.

A pulse is called *chirped* if its intensity temporal envelope has different frequency in each time interval. Firstly, the pulse is stretched in time through strong stretching component. As a result the pulse is positivelly chirped and the peak power decreases in order not to have unwanted phenomena in the amplification medium. After the amplification of the pulse, a compressor is used in order to compress the pulse in time duration equal to the intensity before its stretching, without the chirp. The technique above was introduced by *Gerard Mourou and Donna Strickland* in Rochester University in 1985[22]. For their contribution they won half *Nobel Prize in Physics* in 2018 [23].

The device which causes stretching of the pulse is called *stretcher* and forces the higher wavelengths to exit earlier from its interior (positive dispersion). Then the pulse experiences positive chirp. If the smaller wavelengths come earlier than the higher, the pulse experiences negative chirp (negative dispersion).

The compressor is a device which consists of two elements of chromatic dispersion (prisms or optical gratings) and one or two mirrors. It manages the compression of the pulse and forces the different wavelengths to travel in different optical ways. If the higher wavelengths exit earlier the stretcher, then through the converse procedure the smaller wavelengths will exit earlier the compressor and the pulse obtains its initial time range. However the peak power of the pulse is up to 10^6 higher than the power of the pulse before the amplification.

In the figure below, it is presented a more detailed schematic layout of the technique.

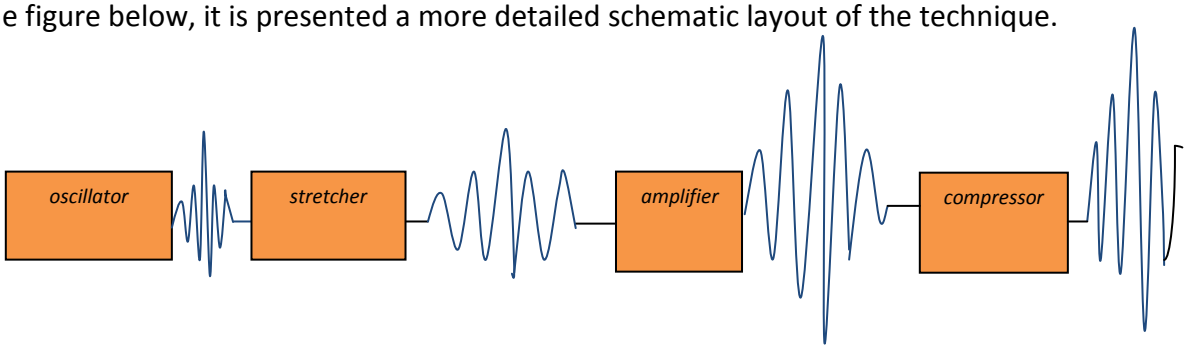

Fig.2.3 Schematic description of CPA technique

Fig.2.4 Layout of femtosecond laser, of multiple amplifiers with two compressors (vacuum compressor of 45 TW and atmospheric compressor of 0.5 TW).

2.2.B FEMTOSECOND SYSTEM GENERAL LAYOUT

The femtosecond 50 TW laser system we use is called *Pulsar* and is divided into three parts: i) front end , ii) amplifiers and air compressor. The layout of the laser system is presented in the picture below.

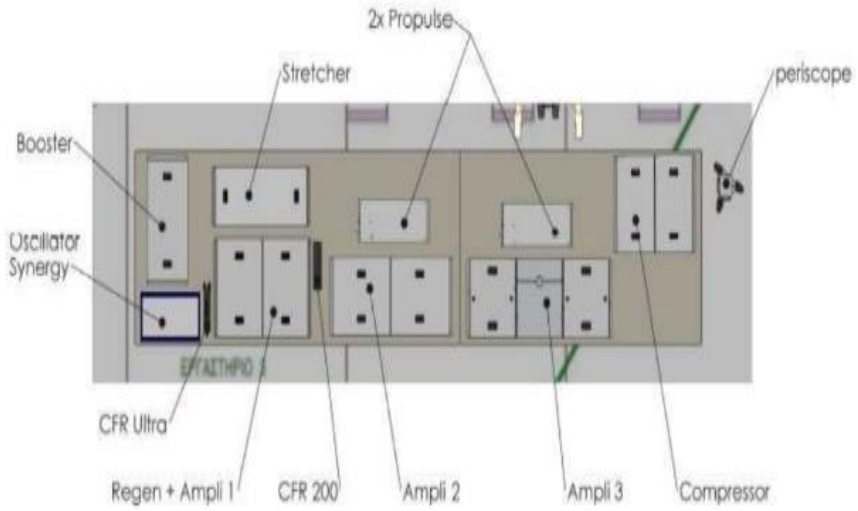

FIg.2.5 Layout of laser system of 45 TW (lab manual)

The pulsed laser system consists of the following parts:

- *Oscillator*
- *Contrast Radio Booster*
- *Stretcher*
- *Regenerative Amplifier (REGEN) and Pre-Amplifier*
- Amplifier of 300*mJ*
- Amplifier 1,5*J*
- *Air compressor*

Furthermore the laser system consists of two *Laser Pumps*:

- A *YAG CFR Ultra* , to pump the *Booster* and the *Regenerative Amplifier*
- A *YAG CFR* 200 to pump the amplifiers of 300mJ and 1.5J
- A *Propulse+* to pump the amplifiers of 300 mJ and 1,5 J
- A *Propulse+* to pump the amplifier of 1,5 J

In addition the laser system consists of two systems of peripheral devices. Specifiacally the systems *Genpulse v3* and *Masterpulse* synchronize all the parts and the pumps and *Control Command* is used in order to control the function of the system.

Oscillator

The *femtosecond laser oscillator* consists of four elements:

- active medium
- *pump laser*
- *Feedback mirrors*, which form an optical cavity.
- *Dispersion compensation optics*.

The *femtosecond* pulses in the oscillator's cavity are generated through *Mode Locking* mechanism.

In fig.2.4 the layout of the oscillator is presented.

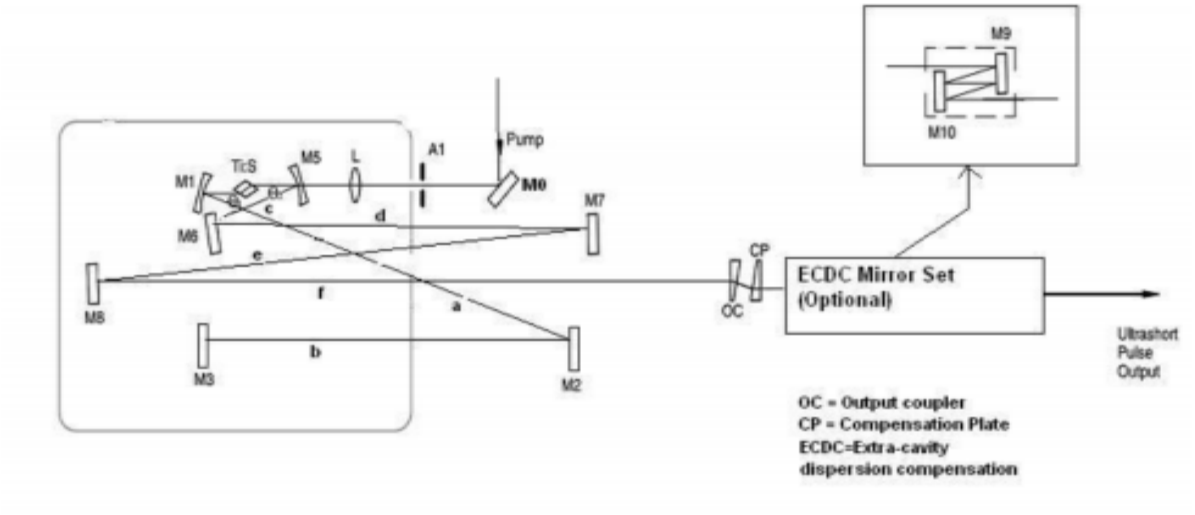

Shortcut	Description	Function
Pump Laser	DPSS 532nm pump source	Seeding the oscillator
M0	HR 532nm mirror	Beam steering mirror
L	lens	Focusing unit for 532nm beam
M1 & M5	Standard Input Coupler	Focus the red beam in the cavity
M6, M7, M8	Chirped mirror in the long arm	Dispersive mirror for steering the red beam in the cavity
M2 & M3	Chirped mirror in the short arm	Dispersive mirror for steering the red beam in the cavity (M3 = endmirror)
OC	Output coupler	Output coupler for the output beam
CP	Compensation plate	Direct the beam after the OC and adjust the dispersion for short pulses
ECDC	Extra cavity dispersion controle	To control the dispersion of the OC and CP to get the shortest pulse

Fig.2.6 Layout of oscillator (lab manual)

The optical Stretcher of the 10 mJ probe fs laser beam

The stretcher consists of a combination of three reflective elements. More specifically it consists of two spherical concentric mirrors. The one is concave and the other one is convex. This combination has perfect symmetry and does not present chromatic aberration because all the optical elements are mirrors [24].

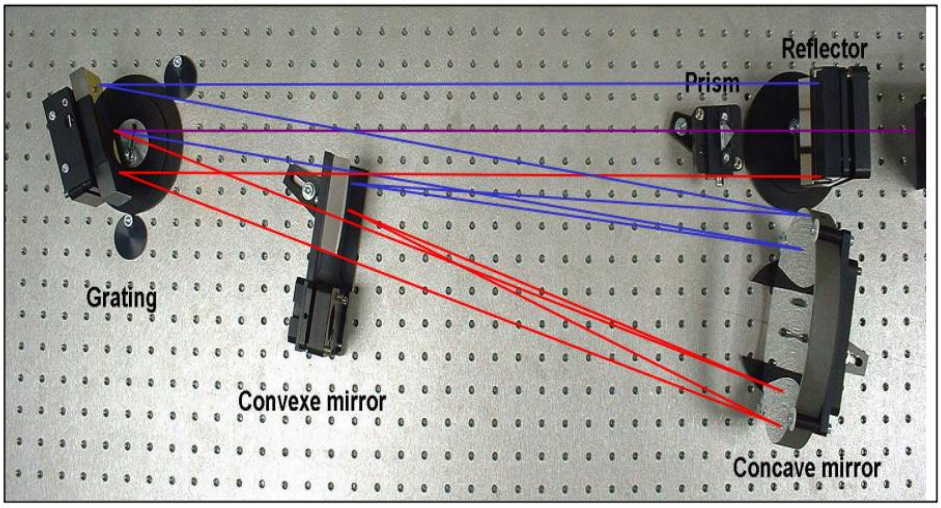

Fig2.7 The layout of Stretcher.

Amplifiers

The first part of amplification includes *regenerative amplifier* which produces stretched pulses of energy 1mJ at frequency 10 Hz. It consists of two *Pocket Cells*. The one is used to induce a stretched pulsed into the cavity and the other one drives the pulse in its maximum energy level.

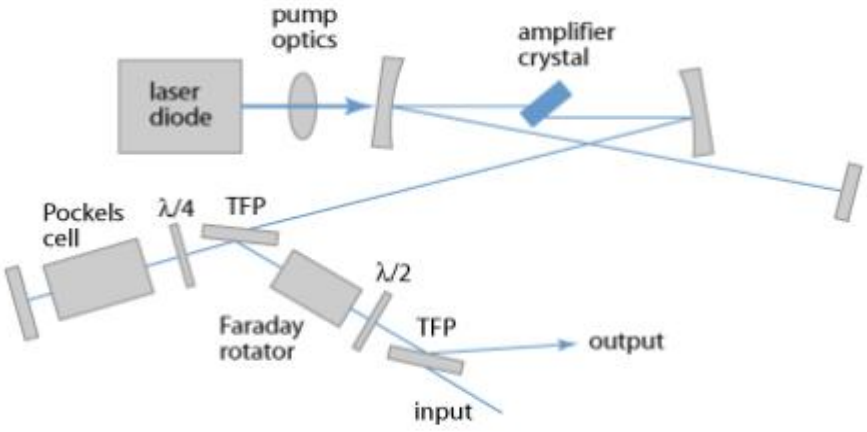

Fig.2.8 Schematic layout of regenerative amplifier.

The amplification of the laser pulse is fulfilled through *multi-pass amplifiers*. An *Nd: YAG CFR200* laser produces gain for the first amplifier, which is called *Pre-amplifier*. The second one is pumped by *Propulse Nd: YAG laser*, of energy 1.2J at 532nm. The main amplifier is pumped by an amount of energy of 5J coming from two Propulse+ Nd: YAG lasers.

Compressor

The amplified pulses are compressed, so that their duration to reach its initial value, before their stretching, with the help of a compressor. Two gratings, with optimum number of slits transmit the wide range of spectrum efficiently. The geometry of stretcher – compressor is adjusted to provide univariable phase dispersion in the total system. For very high output power, the compressor is put in the vacuum chamber in order to protect the laser system from non- linear effects of the air.

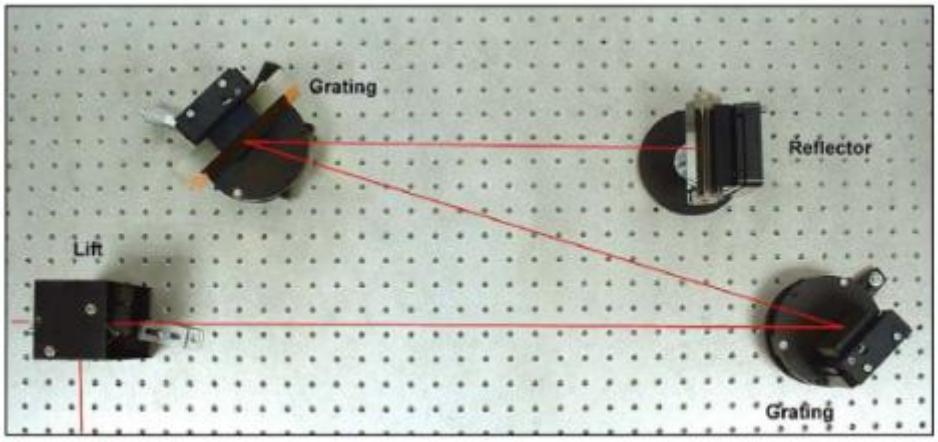

Fig.2.9 Layout of Compressor

2.3 VACUUM TECHNIQUES

Our experimental set up is a semi-infinite cell. Specifically, it consists of a small chamber of gas with pressure a few Torrs, where the harmonics are generated and bigger one, with high vacuum, where they are detected. The laser beam enters the small chamber through a low dispersion optical window to interact with the atoms of the gas and generate the harmonics. The gas enter this small chamber through a needle valve and its pressure is controlled via a manometer. When the harmonics are generated in the small chamber, they enter the bigger one, where there is a high vaccum (~10^{-5} mbars) where their signal is recorded by a detector after their dispression by a optical gratting in certain angles.

The achievement of high vacuum secures both the protection of the MCP detector and the diffraction grating of the experimental set up by impurities and plasma ablation. In addition it secures that the harmonics will reach the detector without being absorbed by gas atoms of molecules, which is between the space of generation and detection.

We can achieve the necessary vacuum with the use of special pumps, which drive the air outside the chamber. There are various categories of pumps. We use a rotary pump to achieve initial vacuum and a turbomolecular to achieve high vacuum about 10^{-5}mbar-10^{-6}mbar, which is necessary for the harmonic propagation and detection.

To achieve high vacuum we use special materials and pump techniques, while with others we clean all the elements of the vacuum chamber and of the pump, in order to avoid air leaks from their interior. Firstly we use the rotary pump to reduce the value of the pressure down to 10^{-2} mbars and afterwards we use the turbomolecular to achieve high vacuum.

The mechanic pumps function with the principle of pumping by using an embolus. The gases have low viscosity. For this reason all the mechanic pumps are rotary and immersed in oil, which acts as sealing. The cycle of the export of the gas happens very quickly and can be repeated by a system, which uses the same axis of motion. The maximum vacuum that can be achieved by these pumps depends on the leak proofness of the system on the points where the axes and the rotator join with the walls of the pump.

The turbomolecular pump is used in order to achieve high vacuum. It has a quick rotator which hits the molecules and catapults them on the exhaust. Most of the turbomoleular pumps create vacuum through several of phases, consisting of quick rotators and a structure with immobile blades. The system compresses the gas. The gas, which is initially trapped, is driven downwards by the rotators. While going downwards, the gas is compressed more and more. This procedure continues up to the point when the gas is pumped from the part on the bottom of the system, by a helping pump.

Fig.2.10 The chamber where HHG occurs.

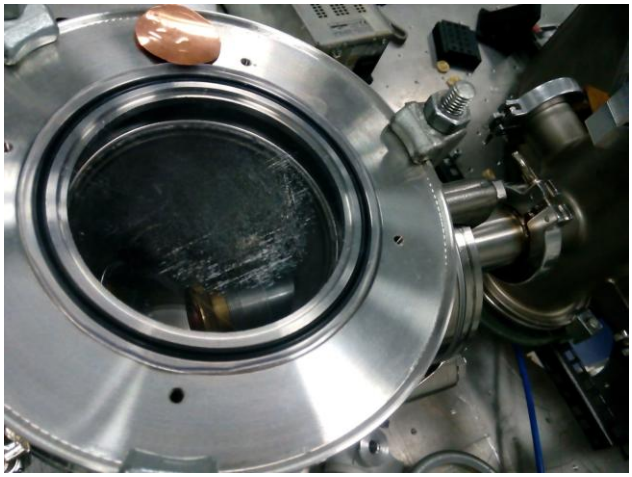

Fig.2.11 Interior of the HHG generation chamber.

2.4 HIGH HARMONIC GENERATION IN LABORATORY

Firstly, laser pulses with energy a few *mJ* and time duration of 25 *fs* are driven with appropriate optics (mirrors and iris) in the focusing lens with focal distance ~ 35 cm. The diameter of the beam before the focusing lens is about 1.2 cm (maximum, at 1/e of the Gaussian) and at the spot of focusing it is estimated to be ~ 50-60μm. The diameter of the laser can be reduced with the use of a controllable aperture. The focusing lens is so thin that it does not stretch the time duration of the laser pulse and thus does not affect our experiment. The lens is located near the entrance window (thin window by *Fused Silica*) of the chamber of generation of harmonics, in order not to create nonlinear effects on it like self-phase modulation, which may destroy the temporal features of the laser pulse. The lens can move in three dimensions with a rotational system of Verner scale. As a result, the beam can be focused on the desirable point in the semi-infinite cell.

After entering the semi-infinite cell, the beam interacts with the atoms of the noble gas. The gas enters the cell through a needle valve which lets us control manually the value of its pressure.

The higher order harmonics, which are generated in our experiment from the interaction of the laser with the noble gas, enter with the fundamental frequency, the second vacuum chamber through a tiny slit generated by the laser itself in copper film of about 0.3 mm thickness. The slit diameter is estimated to be ~50 μm. In the second chamber, there are at high vacuum conditions, the Si-wafer reflectors, the diffraction grating and the MCP detector, which can be moved with a computer controlled electrical microstep motor.

More specifically, the generated harmonics and the laser beam fall on a Si *wafer*. The *Si wafer* is a mirror like a surface made by epitaxial methods, from semi-conductors such as Si, and consists of a semi- conducting surface where the reflection of high harmonics takes place. The arranging of the wafer at *Brewster* angle aims at the achievement of the absorption of infrared radiation and the reflection of the harmonics. The wafer acts as a filter which absorbs the infrared part of the incident radiation and reflects well the harmonics of VUV and XUV region of spectrum.

Afterwards, the reflected harmonics fall on an appropriate *Hitachi flat field-aberration corrected concave* reflection grating. The various wavelengths are sorted as they are diffracted at different angles. After their split, the harmonics fall on the MCP detector, moving with a motor in a straight line. Through a computer we can control the motor.

The moving detector lets us to read with high spatial resolution the signal, because on it there is adjusted a slit that defines a certain dispersion angle. By moving the detector, we select a specific part of the harmonic spectrum, after their diffraction and their focusing on the detector's motion line. The slit lets only a small part of the spectrum to come through it and fall on the MCP. Finally, the signal is recorded by a fast digital oscilloscope.

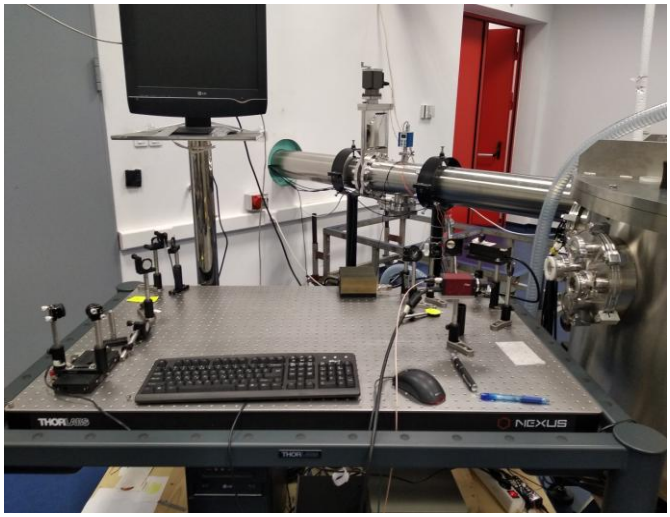

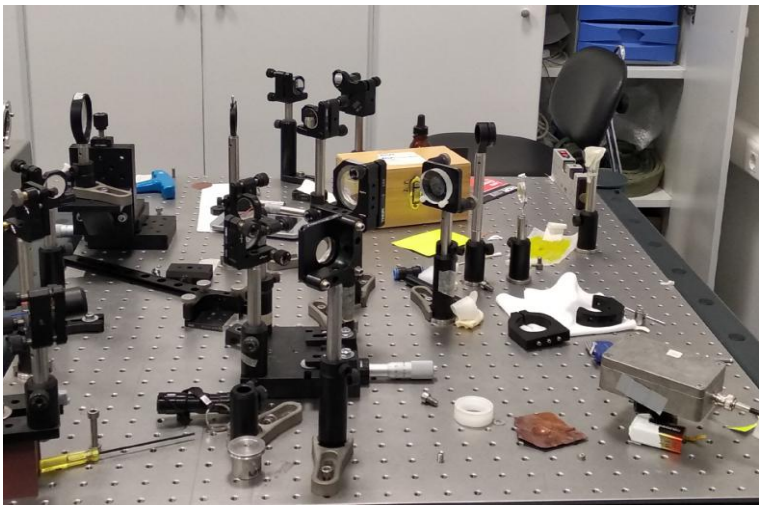

Fig.2.12-2.13 Optics (iris, mirrors) from which the beam passes through when it leaves Amplification chamber.

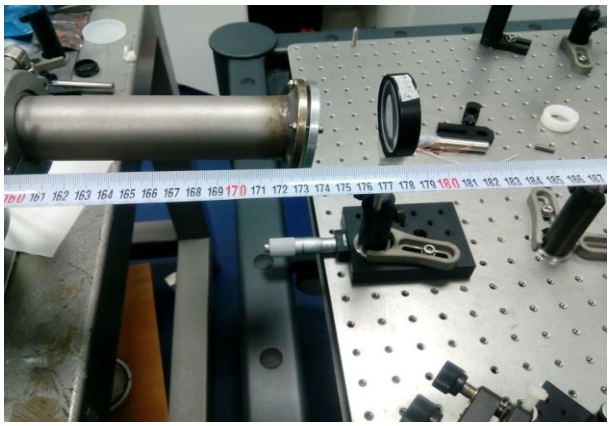

Fig.2.14 The lens which focuses the beam into the semi-infinite cell.

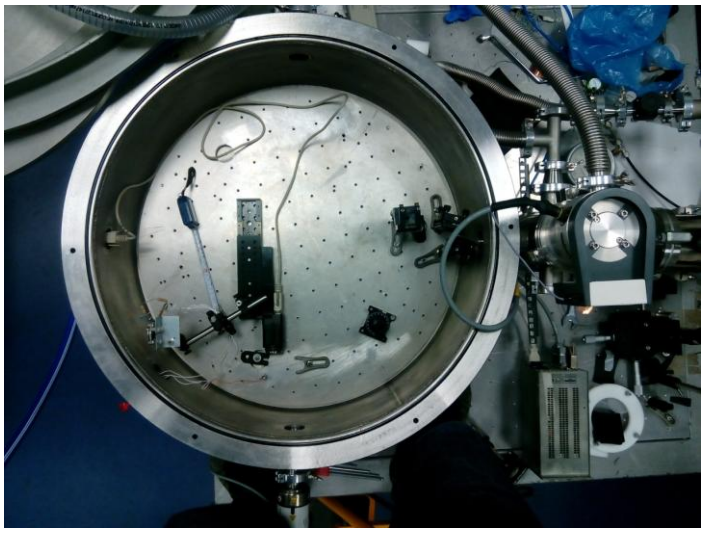

Fig.2.15 Interior of the detection chamber of generated harmonics.Silicon wafers, diffraction grating and MCP detector are shown.

LAYOUT OF EXPERIMENTAL STRUCTURE

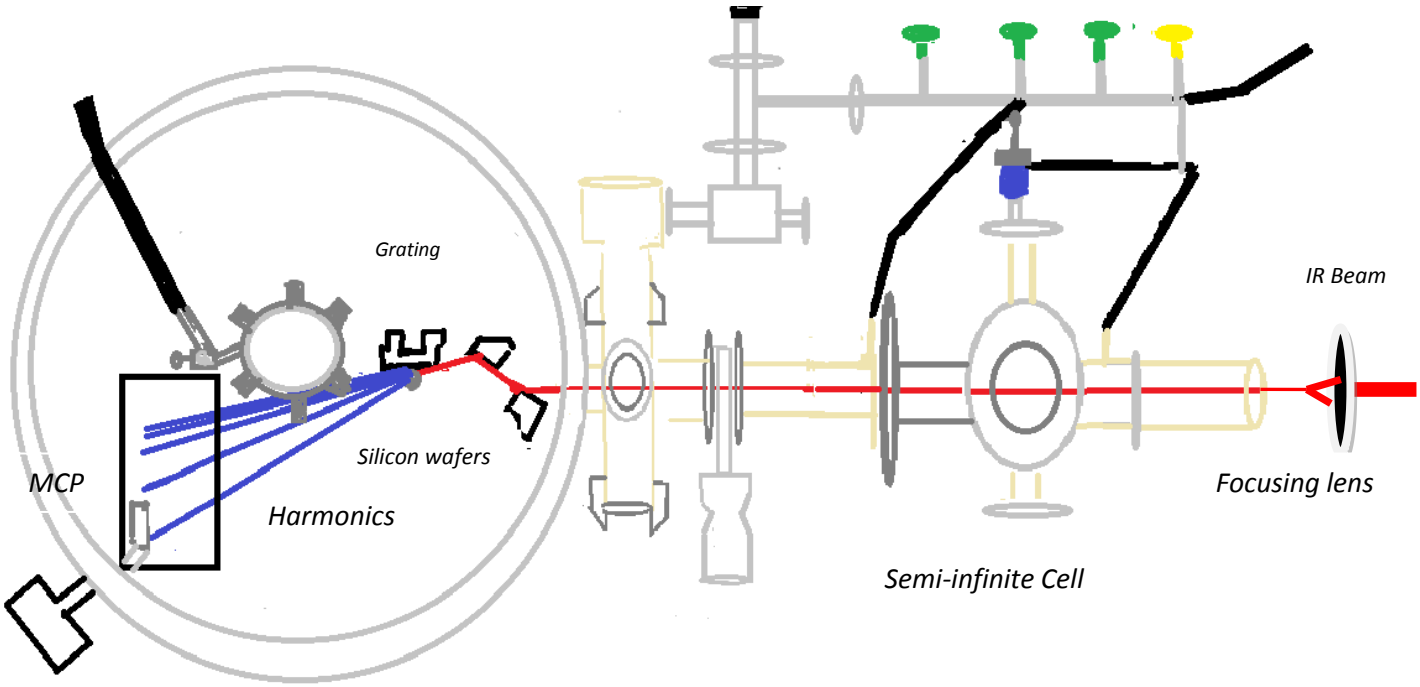

Fig. 2.16 Layout of experimental structure (top view), as it is described in section 2.4

2.5 FLAT FIELD DIFFRACTION GRATING

The diffraction grating is used for the chromatic dispersion of wavelengths of the incident radiation. Its surface is made by a numerous parallel grooves pattern (reflection grating) or slits (transmission grating). It has a substrate made by an optical glass, consisting of numerous grooves, which are created through holographic or lithographic method and are covered with a reflective material, e.g. metal (e.g. Ag, Al or Au)

The equation of the diffraction grating is given by the equation below [25]:

$$\alpha(sinl + sinD) = m\lambda \tag{2.1}$$

Where λ is the wavelength, l is angle of incidence, D is reflection angle, α is groove distance and m an integer number which is the order of diffraction. These angles are defined by the perpendicular to the grating plane. The equation which was derived for 2 grooves is valid for more grooves. In the picture below the reflection of the beam, falling on the diffraction grating is presented.

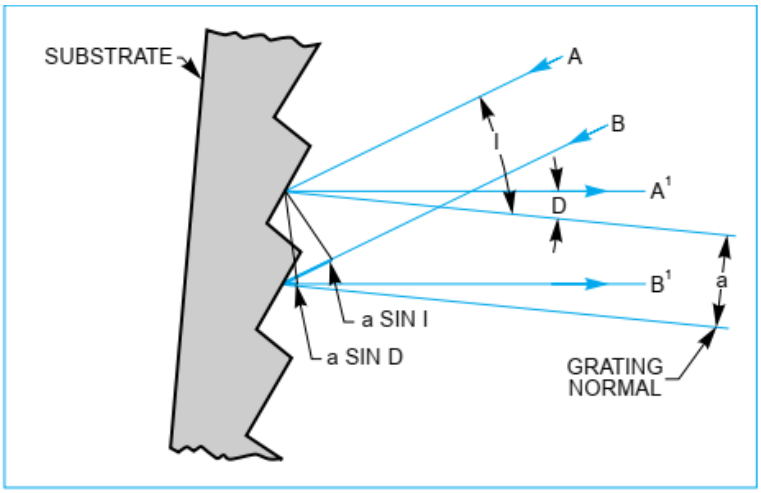

Fig.2.17 Reflection of the beam falling on the diffraction grating [26]

When a light beam, consisting of various wavelengths, falls onto a diffraction grating, each one of them fulfills the equation of diffraction grating. The part of the energy, which is diffracted for each wavelength, is defined as the *efficiency per wavelength.* The efficiency differs per wavelength and can be affected by changing the features of grating, such as angle between grooves, their shape, their depth and the material of the surface of the grating.

The procedure, which is used to alter the features of the grating, in order to achieve the maximum diffraction efficiency, is known in bibliography with the term "*blazing*". The wavelength which corresponds to the maximum efficiency is called *blaze wavelength* and the angle of incidence of the beam is called *blazing angle* [25].

For monochromators (where each counting concerns only a wavelength every time), only the wavelengths which fulfill the Eq.2.1 are diffracted. The rest are absorbed by the material of the monochromator.

The equation for a monochromator is [25]:

$$m\,\lambda = 2\,\alpha\,cos\varphi\,sin\theta \qquad (2.2)$$

m is the order of diffraction**,** λ is the wavelength, φ is the half angle between the incident radiation and the diffracted beam and ϑ is the diffraction angle as a function of the position of the zero order. In Fig.2.19 the diffraction of radiation, falling onto a monochromator, is presented.

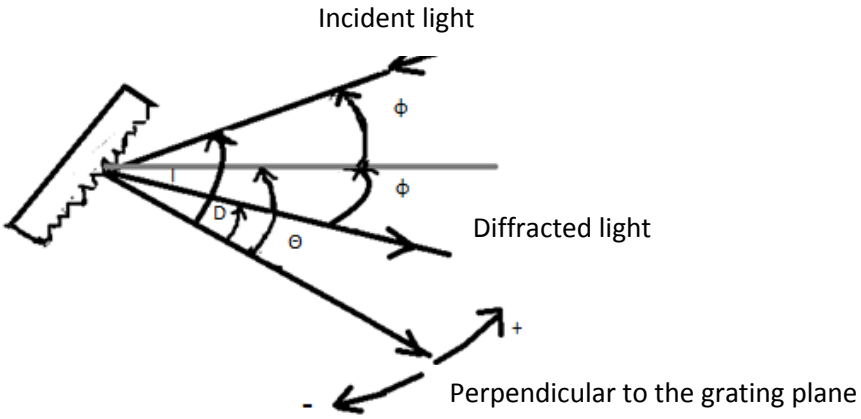

Fig2.18 Diffraction of radiation falling onto diffraction grating

In experiments for harmonic generation, it is often used for a diffraction grating, the *flat field aberration corrected concave grating***.** This type of grating focuses the beam onto a plane surface, which lets their use for linear or 2 dimensional detectors. Their grooves do not have the same distance and are not parallel. They have been designed by a computer in order to optimize the creation of perfect images of entrance slit and of the detector's surface. Furthermore, they consist of numerous of optical openings which are combined with the correction of their aberrations and provide better efficiency of light collection and better ratio of signal - noise.

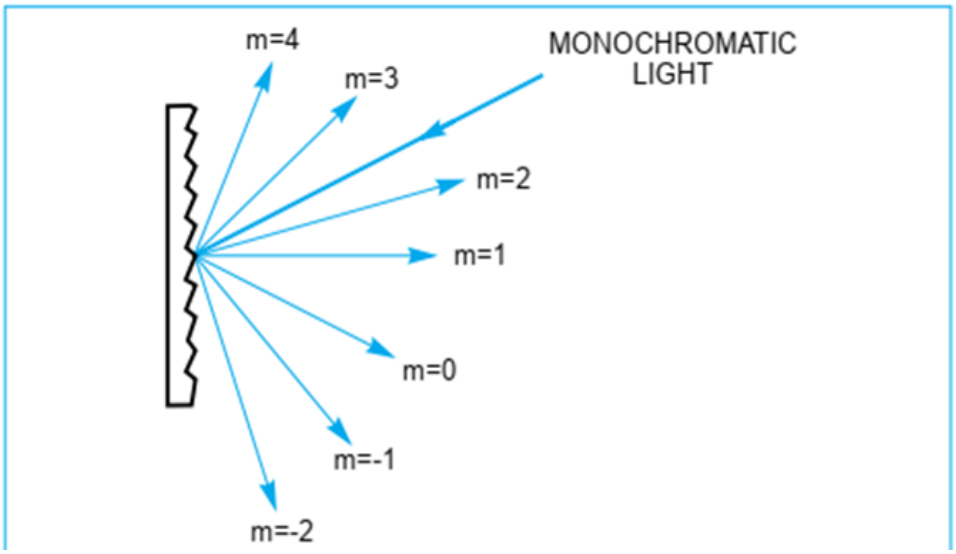

Fig.2.19 Application of grating equation for parallel to the plane beam [25]

The diffraction grating, we use in the experiments is manufactured by the company *Hitachi* and its model code is 001.639. It is made by Pyrex glass and has been covered with silver.

Its dimensions are (50±0.2) mm x (30±0.2) mm x (10±0.2) mm and its camber radius is 5649±20 mm. The area of diffraction has dimensions (48x28) mm but the efficient diffraction area has dimensions (45x25mm) and is suitable for wavelengths of ultraviolet vacuum radiation (22-124nm)[26].The distance between the grooves at the centre is (1/600) mm and the blaze angle is $(3.7\pm0.5)^{o}$. The distances between the grooves are given according to [26] by the equation:

$$\sigma(w) = \frac{\sigma_0}{1 + \frac{2b_2 w}{R} + \frac{3b_3 w^2}{R^2} + \frac{4b_4 w^3}{R^3}} \qquad (2.3)$$

b_2=-8.9 b_3=86.3 b_4=-1349, R is camber radius, σ_0 groove distance at the centre and w the position of the groove.

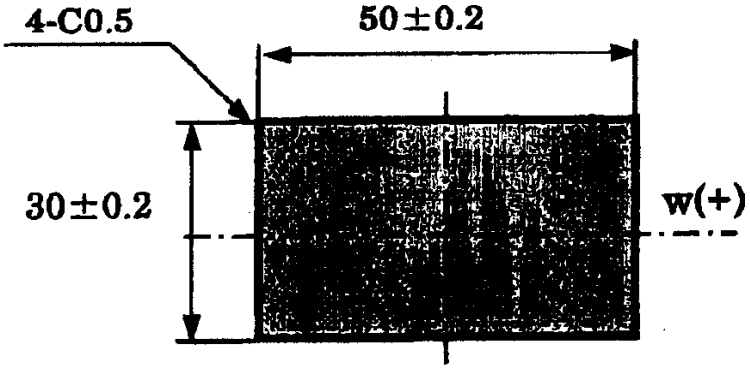

Fig.2.20 Schematic layout of the groove of the grating, where its dimensions are distinct [27].

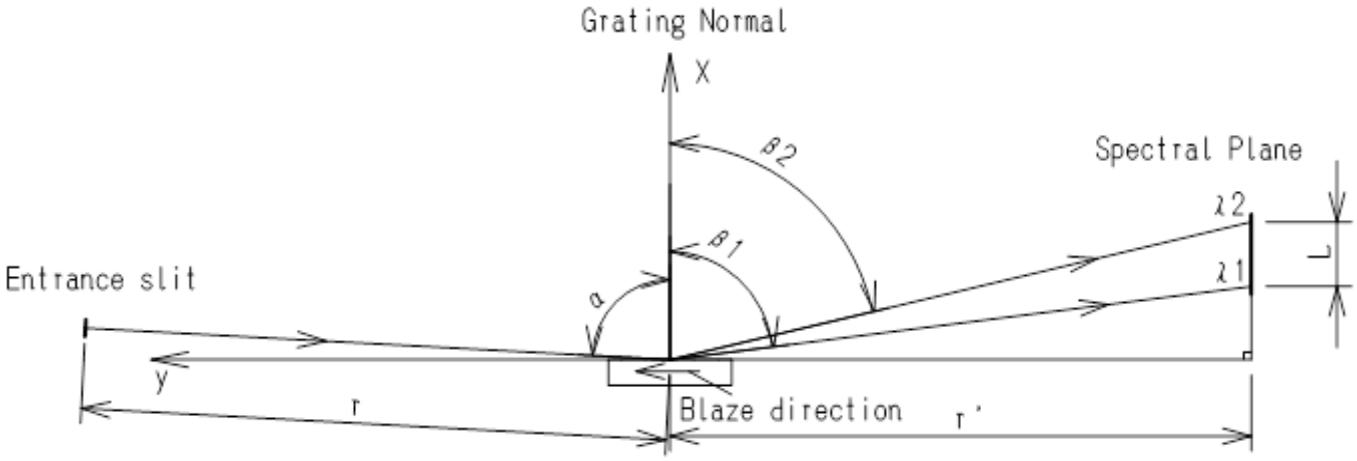

Fig.2.21 Schematic layout of the function of diffraction grating. The values of the angles are given by the manual. α=85.3 r=350mm β_1=-79.56 β_2=-67.26 r'=469mm, L=110.6mm. Wavelength range: 22 - 124nm, blazing wavelength: 31nm [27]

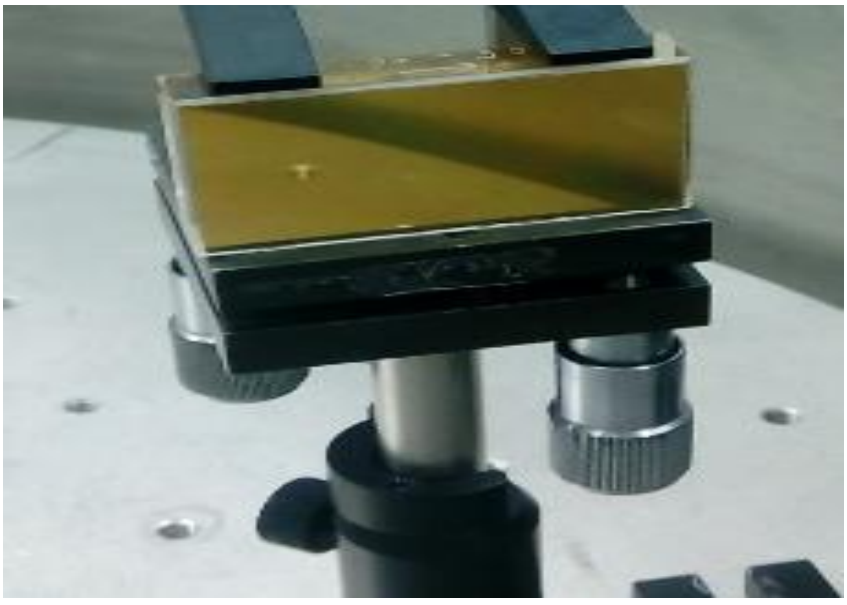

Fig.2.22 Diffraction grating of Hitachi® company (cod: 001.639), which seperates the generated harmonics.

LAYOUT OF DIFFRACTION GRATING AND ITS FUNCTION

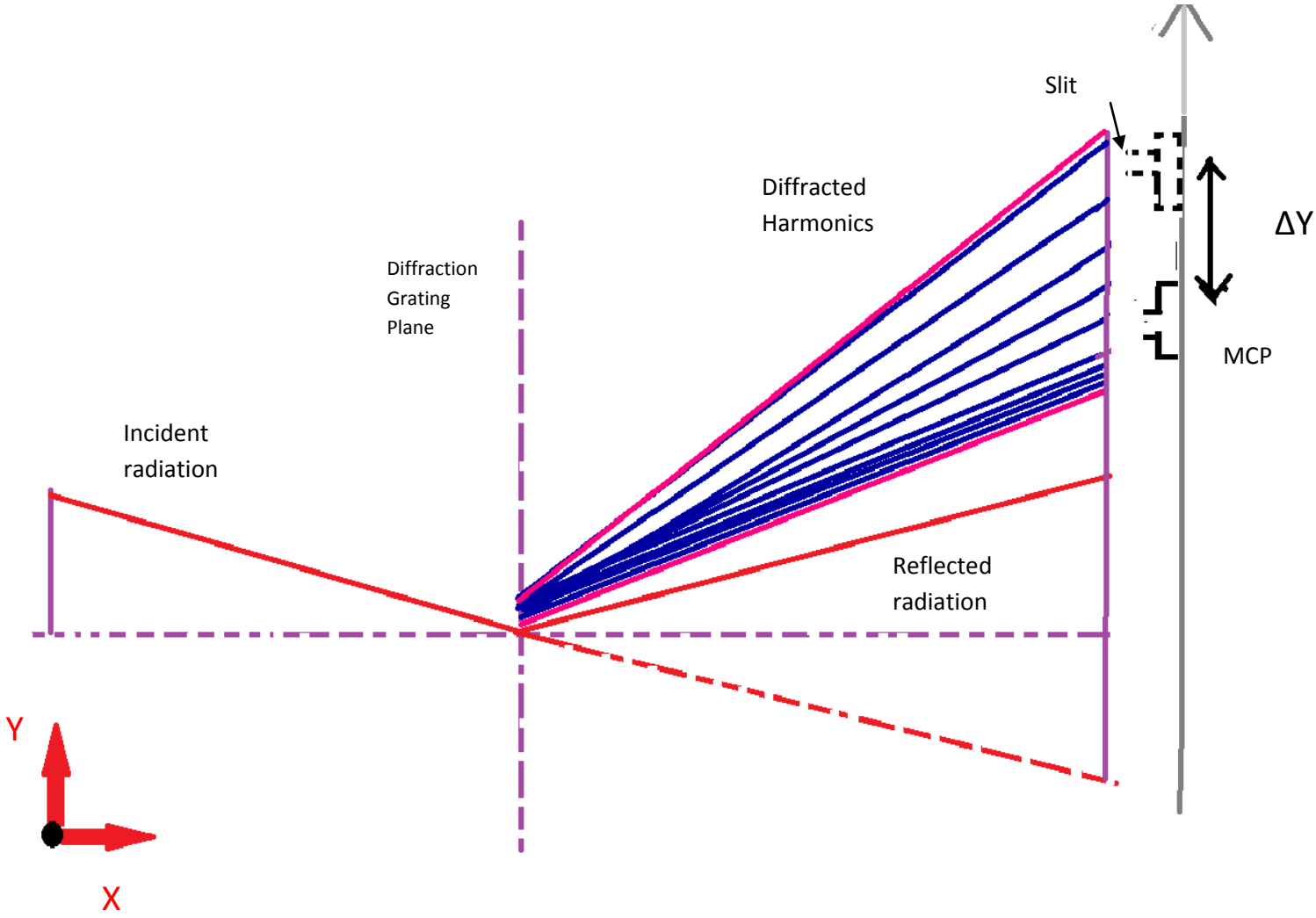

Fig.2.23 Diffraction of harmonics by the diffraction grating. On the right the MCP detector is shown (ΔY is detector's displacement).Through the slit we choose the part of the spectrum that we want to record.

2.6 MICROCHANNEL PLATE DETECTOR (MCP)

MCP detector is used for the detection of particles (electrons, ions, neutrons) and of the incoming radiation of high energy (*UV radiation, X-rays*). It amplifies the signal of the particles or the photons through multi-electron secondary electron emission (avalanche effect).

The existence of many channels which are part of the detector, lets such the detection of the signal as its spectral analysis, as long an appropriate slit is located in the front or a fluorescent monitor is placed at the back, where the electron beams from each channel fall.

Structure of MCP detector

A *MCP* detector is a plate of typical width 2*mm.* It is made by a material of high resistance. It consists of many tiny slits (*microchannels*) leading from the one side of the detector to the opposite. The number of channels is fluctuates between 10^4-10^7. The *microchannels* have typical diameters of the order of few micrometers (about 10μm, 6μm for detectors of high resolution) and are placed in small distance between them, about 15μm parallel the one to the other. In addition they are located on the plate of the detector at small angles ($\sim 8°$) in relation to the normal [28].

The *channel matrix* is usually made of Pb glass in order to optimize the secondary emission. Furthermore the walls of the channel turn into semi-conductors to achieve the refilling of charge by external voltage.

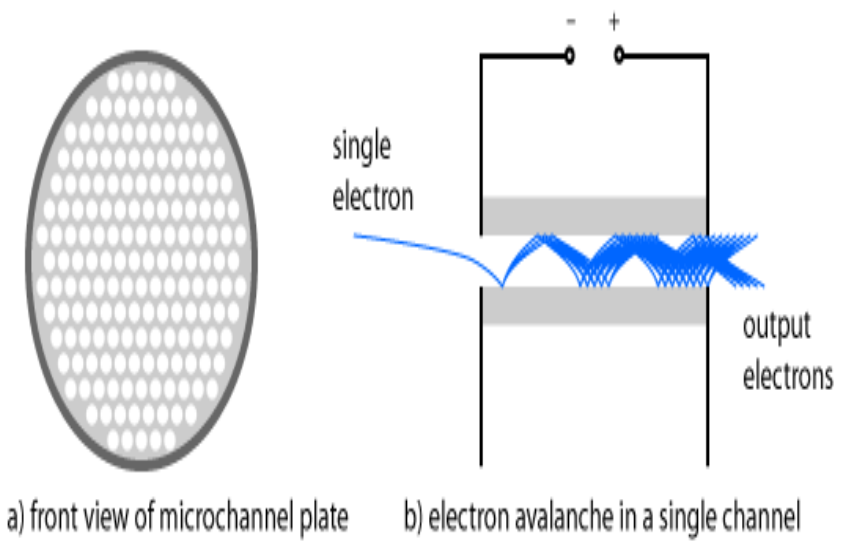

Fig.2.24 Front part of microchannel plate and creation of electron avalanche by a single electron [29].

MCP function

The MCP detector functions as a particle detector, which turns the falling on it particle into an electron avalanche. By applying a strong electric field, vertically to the MCP, each of its channels becomes an *electron multiplier*. A particle or a photon which comes in the channel surely will heat onto its walls, due to the fact the channel shapes an angle with the plate surface. This impact in its turn causes an electron avalanche, which are transmitted through the channel, amplifying the channel by many orders of magnitude. After the avalanche, the channel needs a time period to recover and detect a new signal. The generated electrons exit the channel from the opposite part of the plate where they gather in an anode.

The MCP detector is located into a vacuum chamber (big chamber of the experimental set up) in order to record the signal of the incoming radiation. The particles of the beam, we want to record, come through a thin membrane where the secondary electron emission takes place. Afterwards, they are accelerated by a voltage between the MCP channels. The detector is located out of their trajectory in order not to affect their motion. The number of falling electrons increases by a factor of 10^6 by two multi-channel plates and is transferred in a device of position recording. The incident particle into the channel, hits with high possibility on its walls, as it is located at an angle. This impact results in an *electron avalanche* moving in the interior of the channel, amplifying the initial signal. The efficiency of the amplification depends on the geometry of the MCP and the power of the applying electromagnetic field [28].

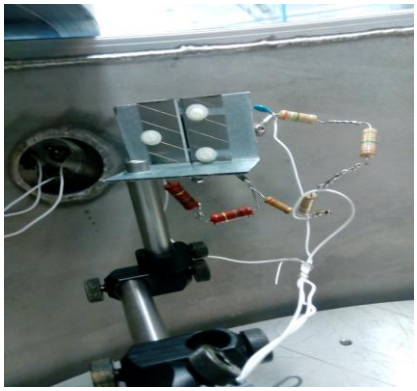

Fig.2.25 The mechanism of moving detector

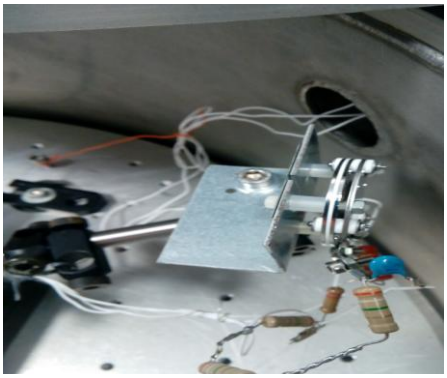

Fig.2.26 Detail of intersection of the decteror we use, to select the harmonics that we want to record.

2.7 OSCILLOSCOPE

The Oscilloscope is a device which lets the observation and the counting of DC and AC electric signals. (Signals are functions of space and time and are represented as *V=V(t)*). It is inset between two spots of the circuit or the source to record electric signals. The oscilloscope has very different resistances in its entrance (50 Ω or MΩ).

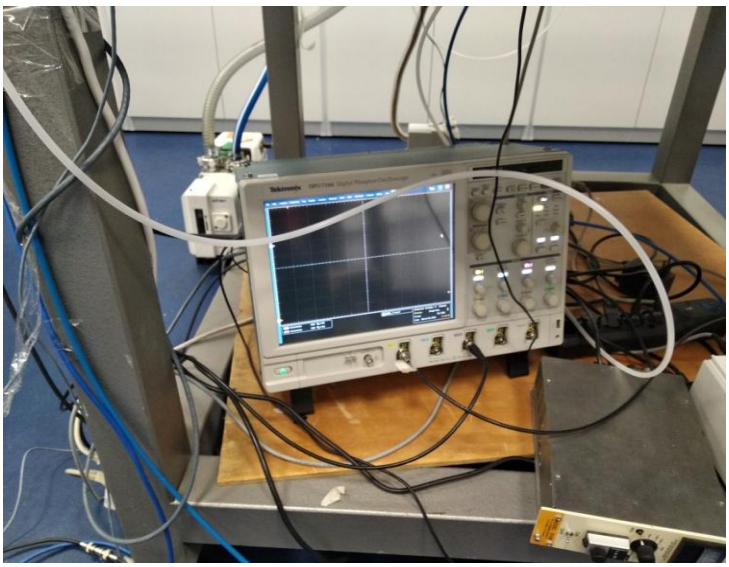

Fig.2.27 The oscilloscope we use in the laboratory

In our experiment we use a digital oscilloscope for the recording of the signal of the harmonics which fall onto the MCP detector. We define the MCP voltage in about 1.5kV in order to receive enough signals in the oscilloscope using the 50Ω input resistance. Note that the MCP electric signal is in the order of few tens of nanoseconds. Without the laser but having charged the MCP with its high voltage we observe sudden random fast signals in the oscilloscope monitor. Before the recording of harmonic signal we observe that a current of low power appears in the oscilloscope monitor. This current is called *dark current* and is owed to the random generation of electrons and holes in the *depletion region.* The *dark current* is the main source of noise in our signal.

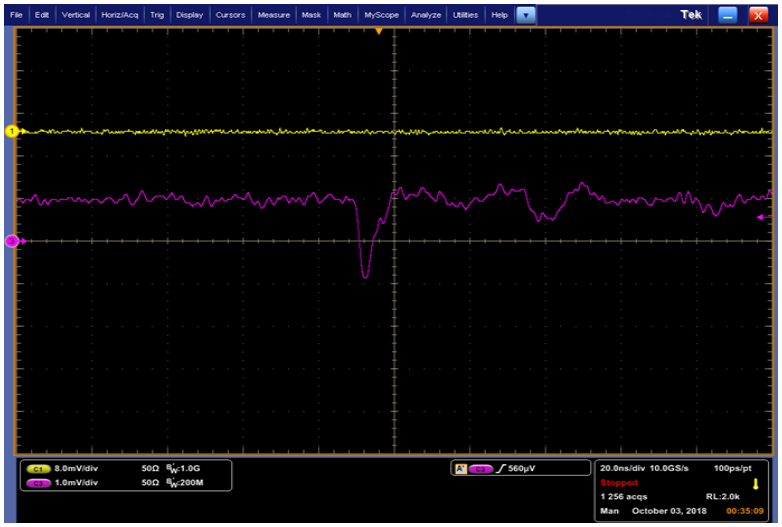

Fig.2.28 Dark current in the monitor of the oscilloscope before the recording of the harmonic signal

Furthermore, for the prosecution of the experiment it is necessary to know when we will activate the system in order to receive a counting of the harmonic spectrum (*trigger system*). This goal is achieved through a photodiode which records when the reflected part of the beam, by the lens, falls onto it.

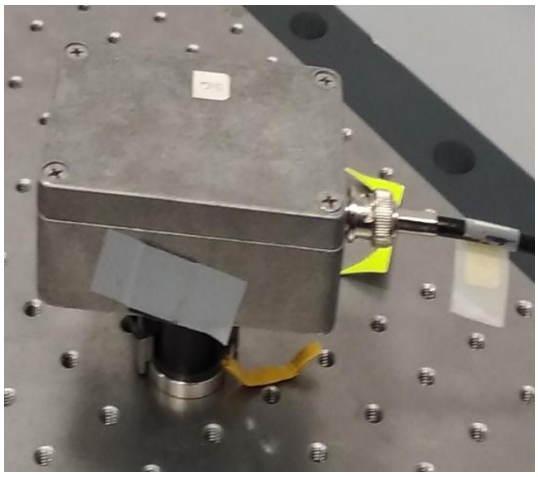

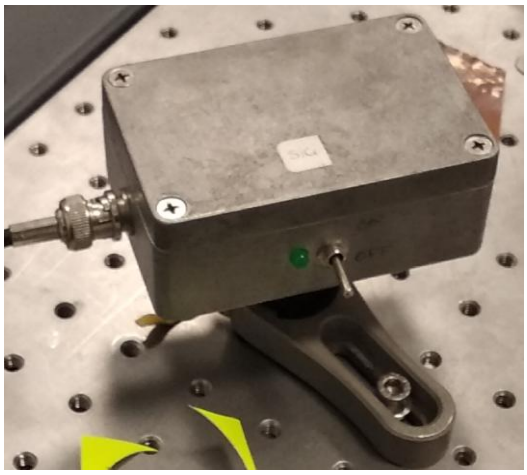

Fig.2.29-2.30 The photodiode we use in the experiment.

2.8 RECORDING OF HARMONIC SPECTRUM

The spectrum of the harmonics which fall on the detector is recorded by software developed for the needs of the experiment. Only the odd harmonics are recorded due to the spherical symmetry of the atoms of the noble gas. The system of the diffraction grating functions in the range of wavelengths 22-124nm. We derive the scientific results by the computing program and we save them directly in an *Excel* file. In one column the amplitude of the harmonic intensity is saved and in another one we save the values of the displacement of the MCP which later can be transformed in wavelength.

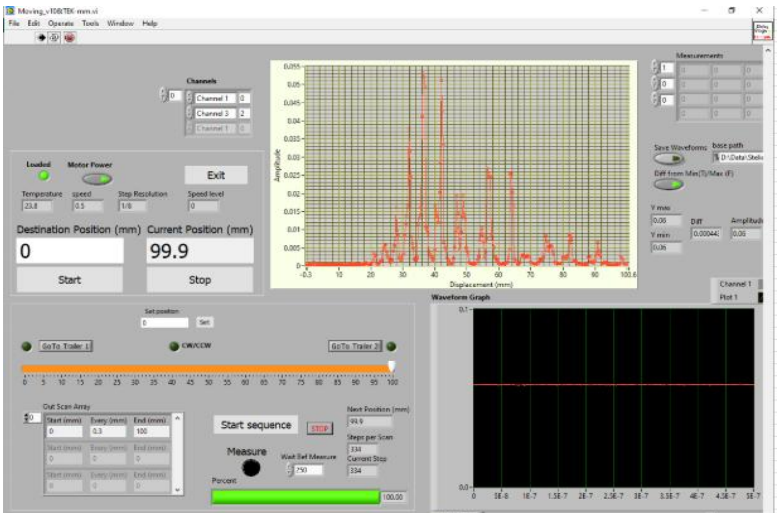

Fig.2.31 Desktop of the computing program of harmonic recording.

CHAPTER3. PRESENTATION AND ANALYSIS OF EXPERIMENTAL RESULTS

3.1 INTRODUCTION

In this chapter of the master thesis, the experimental results are presented in relation to high harmonic generation in a semi-infinite gas cell. More specifically, the harmonic signal as a function of their wavelength (power spectrum) is measured experimentally. A computing program of recording is made to measure the harmonic oscilloscope signal of the harmonics as a function to the displacement of the detector's slit. Afterwards through a procedure which is described in section 3.1 we convert the horizontal axis from displacement units to wavelength units.

Spectra of three gases are measured, namely: Argon (Ar), Neon (Ne), Nitrogen (N) at conditions of same laser intensity in the cell and same pressure of the each gas. For the gases Argon and Neon also, the focus position of the beam according to the active medium does not change. There is a comparison between the spectra of the gases and the interpretation of the differences of them is attempted.

Later, spectra of Argon at various pressure and focus positions are presented in order to investigate the way that these two variables affect the spectrum of emitted harmonics. We also take into consideration the variation of amplitude of harmonic orders 19 to 29 as the pressure of Argon and the focus position of the beam into the cell varies.

3.2 CALIBRATION OF MONOCHROMATOR

In this section, the procedure we follow to calibrate the monochromator, is described. Specifically, the necessary steps in order to correspond a specific value of the detector's displacement to a wavelength of *XUV* radiation are described. In the picture below, the diffraction of radiation which falls onto the grating is presented.

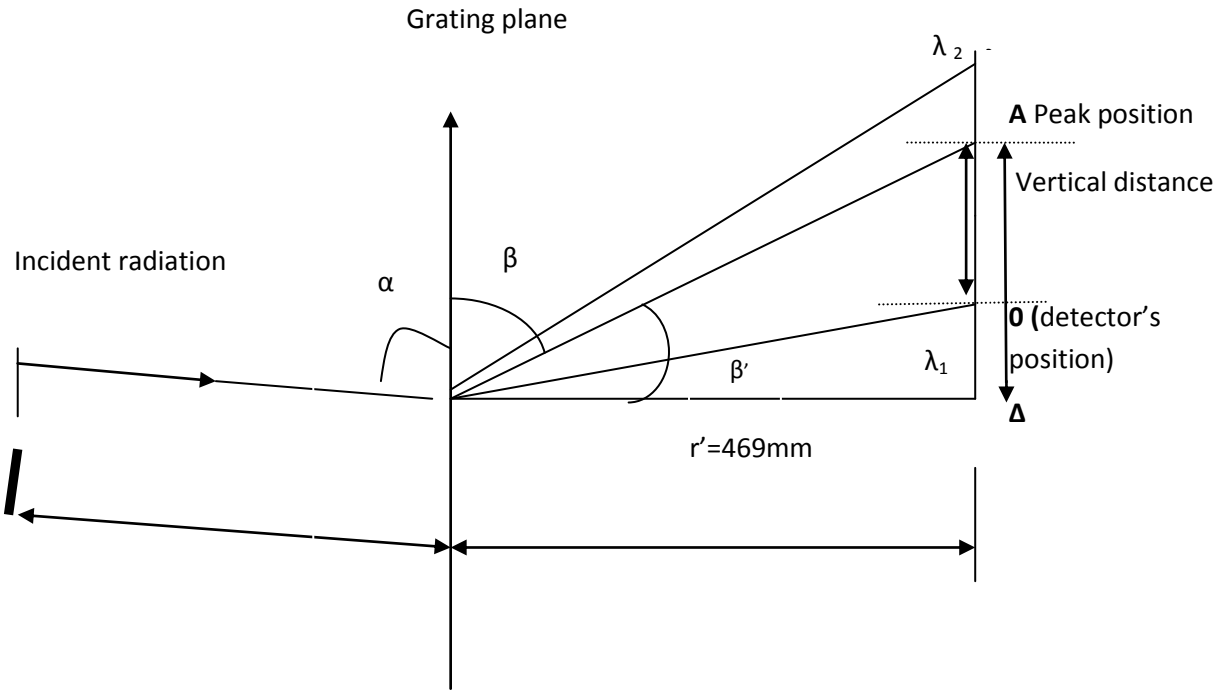

Fig.3.1 Diffraction of the harmonics by the diffraction grating.

In Fig.3.1 with *0* we note the position of the detector. *0A* is the position of each peak of XUV radiation, which falls on the MCP detector. With *OΔ* we mark the difference between vertical distance-peak positions. With *α* we state the angle between the incoming radiation and the normal to the diffraction grating (α=85.3^{o}).

In the following table we present the expected position, that every harmonic of fundamental beam (λ_0=810nm), is diffracted.

λ_0=810nm	Harmonic order	Nm	β(diffraction angle)	Vertical side(mm)	Distance from λ_1(mm)	Distance of consecutive harmonics (mm)
	3	270	56.578	309.5	223.1	
	7	116	68.004	189.5	103.0	120.1
	9	90	70.499	166.1	79.7	23.4
	11	74	72.261	150.0	63.6	16.1
	13	62	73.588	138.1	51.7	11.9
	15	54	74.631	128.9	42.5	9.2
	17	48	75.477	121.5	35.1	7.4
	19	43	76.182	115.4	28.9	6.1
	21	39	76.779	110.2	23.7	5.2
	23	35	77.293	105.8	19.3	4.4
	25	32	77.741	101.9	15.5	3.8
	27	30	78.136	98.5	12.1	3.4
	29	28	78.487	95.5	9.1	3.0
	31	26	78.801	92.9	6.4	2.7
	33	25	79.085	90.4	4.0	2.4
	35	23	79.343	88.3	1.8	2.2
	37	22	79.578	86.3	-0.2	2.0
	39	22	79.558	86.4		
Diffraction range: 22-124nm	λ_1	22	79.558	86.4	0.0	0.0
	λ_2	124	67.255	196.6	110.18	-110.18

Tab.3.1 Expected position, that every harmonic of fundamental beam (λ_0=810nm), is diffracted.

The diffraction angles for each wavelength are calculated by the equation:

$$\beta_m = \arcsin\left(\frac{m\lambda}{d} - sina\right) \quad (3.1)$$

d=1667*nm* is the distance between two consecutive slits of the grating

In the picture below, a spectrum for gas Argon at pressure 30 Torr and focus position z_f=0mm, is presented. The procedure we use to correspond each value of the displacement of the detector to a wavelength. The same procedure is followed for all the spectra which are presented in the Master Thesis.

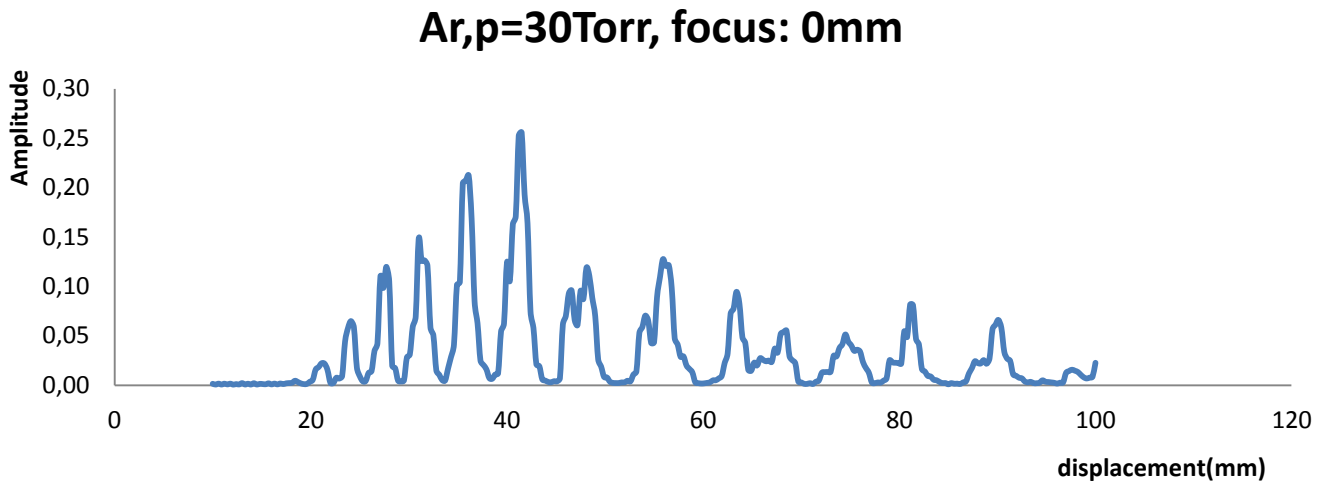

Fig.3.2 The spectrum of the amplitude of each harmonic as a function of the detector's displacement (Amplitude-displacement).

From Fig.3.2 we note the position of the first seven peaks (from the left side).

We calculate their differences and we compare them to the differences of the harmonics which are diffracted by the grating (q.v. Table 3.1). We observe with which harmonic differences they fit better and we correspond each peak position to the *Vertical Side* that it diffracts theoretically. We calculate the difference OΔ.

We calculate the mean value of the differences, which we add to each peak position. By this way we calculate the experimental vertical distance which corresponds to each peak. From the geometry of Fig.3.1 we calculate angles β, β'.

From Eq.3.1 we derive the wavelength:

$$m\lambda = d(sina + sin\beta) \quad (3.2)$$

The angles *α, β* have opposite sign. m=1 (1st diffraction order)

By following the procedure above we correspond each peak position to a specific wavelength. This correspondence is shown at Table3.2

Peak position(mm)	Difference of consecutive peaks(mm)	Theore-tical Vertical Side-V.S. (mm)	Difference V.S – peak position (mm) **ΟΔ**	Experime-ntal Vertical Side (mm)=Peak Position+ M.V.	tanβ= $\frac{\text{Exp. V. S}}{r'}$ $r': 469mm$	β°	β'° (90-β)	m=1 λ=d(sinα+sinβ') d=1667nm α=85,3° (incident angle)
41.5	-	-	-	-	-	-	-	
35.8	5.7	110.2	74.4	110.2	0.234	13.17	76.83	38.17
31.3	4.5	105.8	74.5	105.7	0.225	12.68	77.32	34.99
27.6	3.7	101.9	74.3	102	0.217	12.24	77.76	32.23
24.1	3.5	98.5	74.4	98.5	0.210	11.86	78.14	29.92
21.1	3	95.5	74.4	95.5	0.2036	11.51	78.49	27.86

M.V. =74.4

Tab.3.2 Correspondence between peak position-wavelength.

From Eq.3.2 and the geometry of the problem (q.v.3.1) we derive Eq.3.3 which gives the wavelength, corresponding to each value of the detector's displacement.

$$\lambda = 1667(0.9966 - \frac{469}{\sqrt{(M.V. + disp.)^2 + (469)^2}}), m = 1 \qquad (3.3)$$

With the method above, we correspond each value of the detector's displacement to a specific wavelength. In the picture below the horizontal axis of Fig.3.2 is converted into nm.

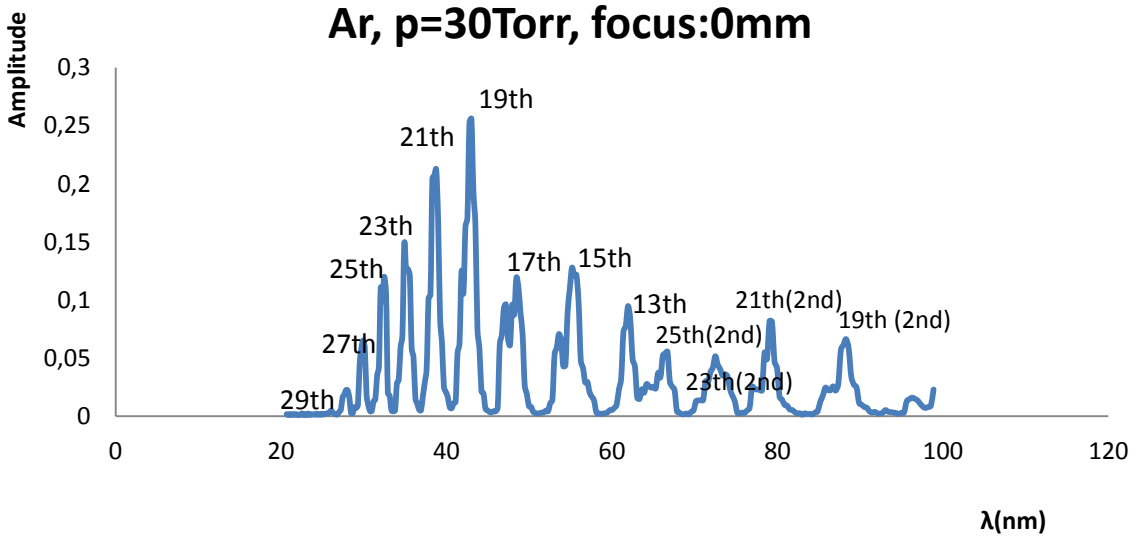

Fig.3.3 Spectrum of XUV radiation, after the conversion of the detector's displacement into wavelength units.

In Fig.3.3 we observe that up to the 13th harmonic, the theoretical values for the wavelengths of the harmonics match with accuracy of a tenth of nanometer with the values that we corresponded following the procedure above. After 13th harmonic the peaks do not correspond to harmonics of 1st diffraction order. They correspond to 2nd diffraction order. The equation that concerns the 2nd diffraction order is:

$$m\lambda = 1667(0.9966 - \frac{469}{\sqrt{(M.O.+disp.)^2 + (469)^2}}), m = 2 \quad (3.4)$$

Peak wavelength (Fig.3.3)	Harmonic of 2nd diffraction order
66.70=2x 33.35(32nm)	25th
72.48=2x 36.24(35nm)	23th
79.03=2x 39.51(39nm)	21th
88.28=2x 44.14(43nm)	19th

Tab.3.3 Correspondence of the peaks of the spectrum to the 2nd diffraction order harmonics.

In Tab.3.3, in the parenthesis we note the theoretical value of the wavelength for each harmonic.

3.3 PRESENTATION AND COMPARISON OF THE SPECTRA FOR GASES ARGON (AR), NEON (NE), NITROGEN (N)

In the figures below, the intensity of the harmonics (amplitude as a function of wavelength) for three different gases is presented: Argon, Neon and Nitrogen at pressure **p=50Torr.** Also, for gases Neon and Argon the focus position of the beam is the same (z_f=+3mm on the pinhole). The focus position, we receive clear spectrum for Nitrogen is z_f=+8mm.

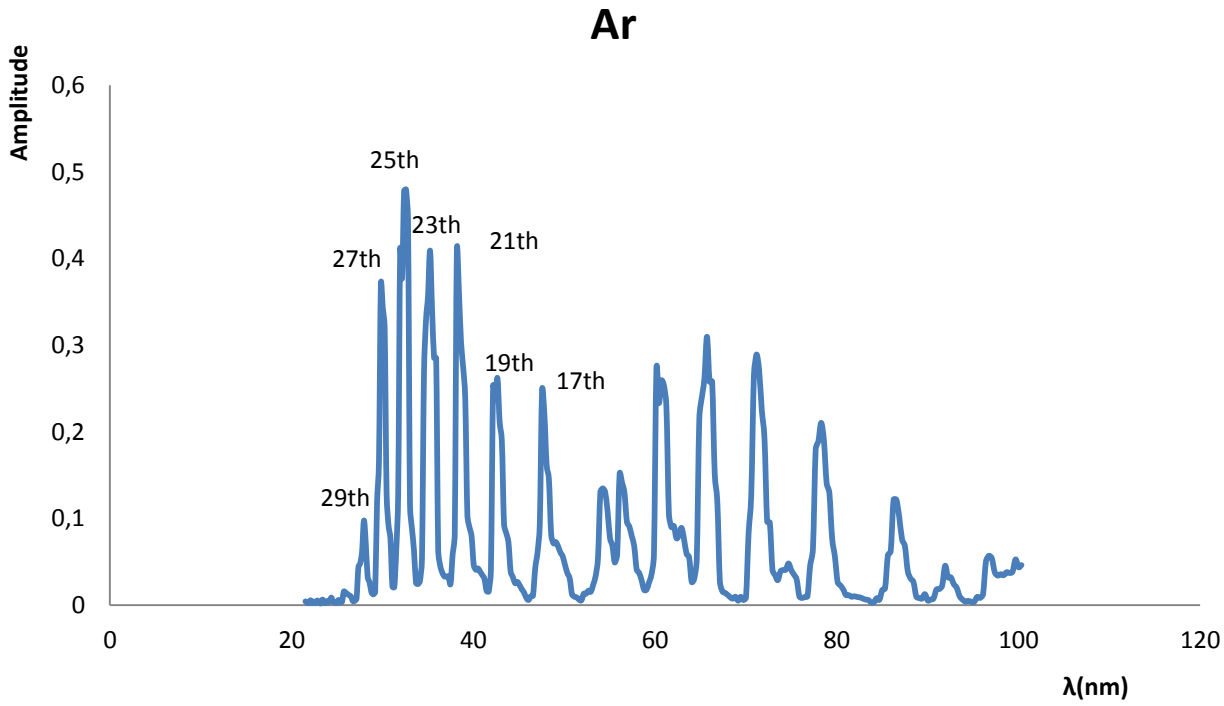

Fig.3.4 Amplitude of XUV radiation for Argon at p=50 Torr and focus position z_f=+3mm.

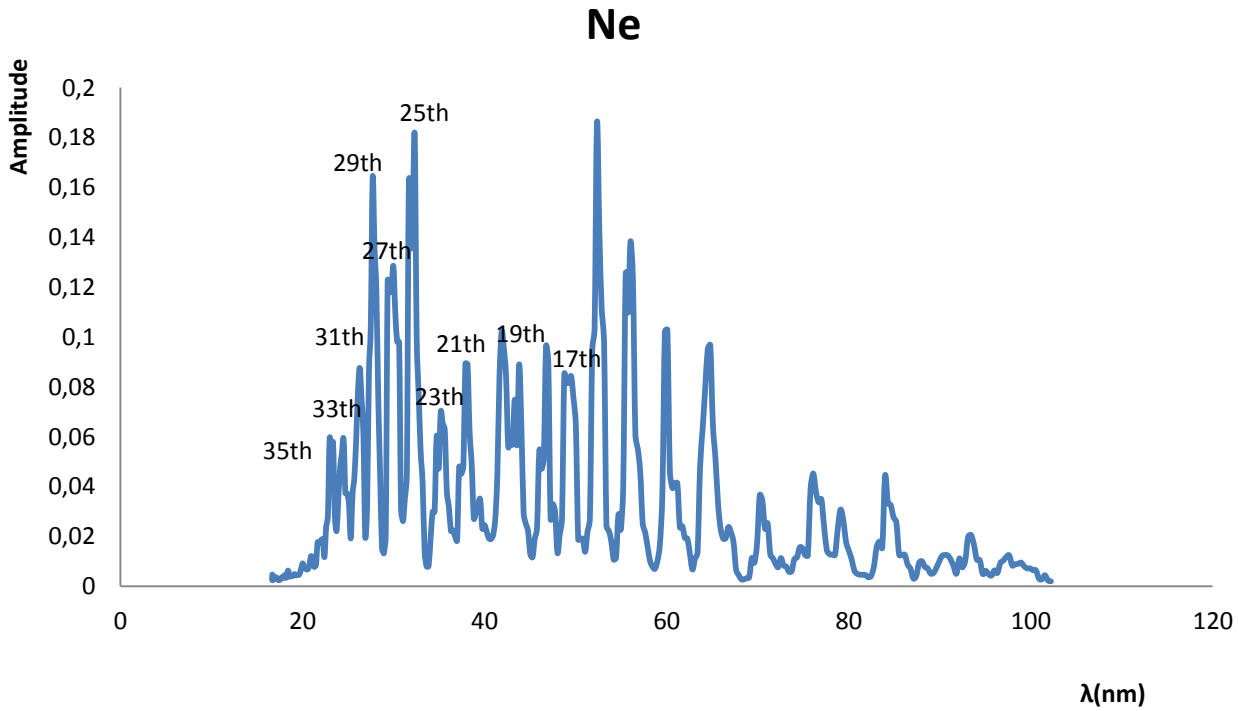

Fig.3.5 Amplitude of XUV radiation for Neon at p=50 Torr and focus position z_f=+3mm.

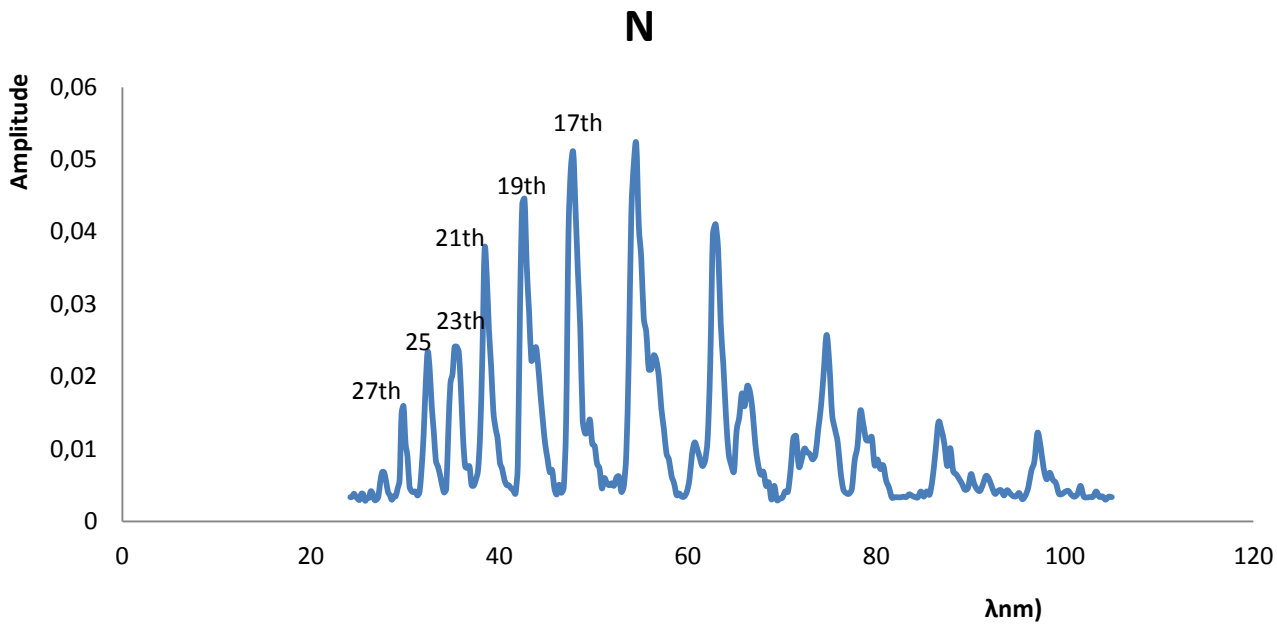

Fig.3.6 Amplitude of XUV radiation for Nitrogen at p=50 Torr and focus position z_f=+8mm.

In the table below the values for the harmonic amplitudes for the gases Ar, Ne and N, are presented, at pressure 50 Torr.

Harmonic order	Amplitude (Ar)	Amplitude (Ne)	Amplitude (N)
35th	-	0.059	-
33th	-	0.058	-
31th	-	0.087	-
29th	0.098	0.104	-
27th	0.371	0.123	0.015
25th	0.478	0.181	0.020
23th	0.409	0.065	0.023
21th	0.409	0.062	0.038
19th	0.252	0.089	0.044
17th	0.247	0.085	0.051

Tab.3.4 Normalized value of harmonic amplitude for gases Argon (Ar), Neon (Ne), Nitrogen (N) at p=50 Torr.

COMMENTS

I) Experimental cut off frequency ω_c

We notice from the diagrams of amplitude-wavelength above, for these three gases, that the experimental cut-off frequency differs for each gas. More specifically, the observed cut-off frequency for Neon (35^{th} harmonic) is clearly higher than the corresponding for Argon (29^{th} harmonic). In addition, the cut-off frequency for Nitrogen is even lower (27^{th} harmonic).The behavior of the spectra of the three gases as regards the area of frequencies where the cut- off takes place, is expected. We expect to have higher cut- off frequency in Ne than in Ar and N.

From Eq.1.8 we conclude that the cut-off frequency is analogous to the ionization potential I_p and to ponderomotive energy U_p. Due to the fact that the intensity *I* of the fundamental laser beam is almost the same for the three gases (~1,2mJ per pulse for Ar, Ne and 1.08mJ for N), the cut- off frequency presents differences because of the different values of ionization potentials of the three gases. We know that:

$$I_{p,N}<I_{p,Ar}<I_{p,Ne}\ (\ I_{p,N}=14.5eV,\ I_{p,Ar}=15.8eV,\ I_{p,Ne}=21.6\ eV)$$

We note at this point that the differences can be much higher, but not be observed due to the detection system, as the diffraction system functions efficiently up to 22nm (37^{th} harmonic).

II) Differences in Harmonic Amplitude for the three gases due to the absorption of radiation.

From the three diagrams (Fig3.7-9) we notice that the amplitude of harmonics 17-27 differs significantly for each gas. In Argon the harmonics have higher amplitude than the corresponding harmonics in Neon and Nitrogen. A factor that could be responsible for this is the different absorption of the gases for the various wavelengths. For wavelengths corresponding to harmonics 17-29 the Argon has higher transmission than Neon and Nitrogen.

After their generation by the fundamental beam, the harmonics are absorbed by the atoms of the gas in the semi-infinite cell. The absorption, even when phase matching conditions are fulfilled, is a factor that limits the length of the medium which contributes in the microscopic field of harmonics. The calculation of transmission as a function of the wavelength happens through the application which is available in *https://henke.lbl.gov/*. We consider approximately that the distance that radiation traverses from the point of harmonic generation up to their entrance in the high vacuum chamber (where the detection takes place) is of the order of 3mm, the temperature is constant at 295K (room temperature) and the pressure is 50 Torr.

In Fig.3.7-3.9, the dependence of transmission *T* (*T*=1-*A*, *A*: absorption of radiation) as a function of wavelength in nm for gases Argon, Neon, Nitrogen, is presented.

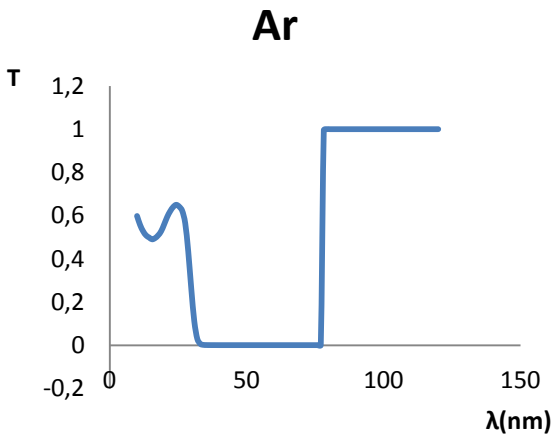

Fig3.7 Transmission of gas Argon as a function of wavelength in nm.

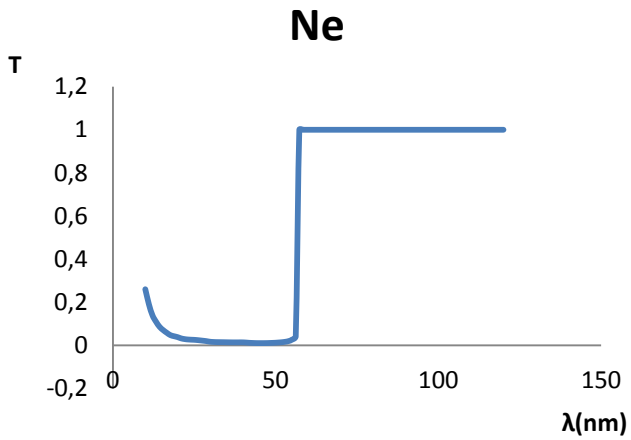

Fig3.8 Transmission of gas Neon as a function of wavelength in nm.

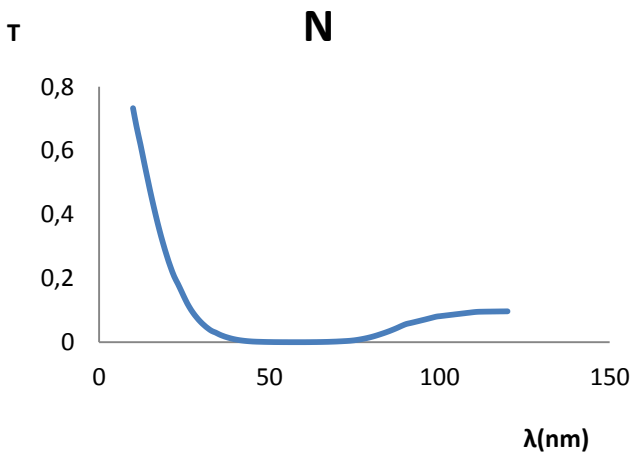

Fig3.9 Transmission of gas Nitrogen as a function of wavelength in nm.

III) Differences in harmonic amplitude of the three gases due to the different first ionization potential and the energy per pulse of the fundamental beam.

As it was mentioned before, the three gases have different ionization potentials. Neon is the gas with highest ionization potential. Practically, that means that harmonic generation is more difficult than in Argon for the same conditions of intensity of the laser beam and focusing in the semi-infinite cell. Consequently, with the same intensity of laser beam (energy per pulse 1.2mJ), harmonics of same order have noticeably lower amplitude in Neon than in Argon.

In Nitrogen the corresponding harmonics present even lower value. A possible explanation of this behavior could be attributed to the lower energy per pulse of the laser beam of 810nm, which we use to generate harmonics in Nitrogen. The energy of fundamental, for the harmonic generation by Nitrogen atoms was 1,08mJ.

In addition according to ***Heyl et al.*** [30], inside the focus of laser beam, the pressure in which perfect phase matching is fulfilled, is given by the Eq.3.5

$$p = p_0 \frac{\lambda^2}{2\pi^2 {w_0}^2 \Delta\delta (1 - \frac{\eta}{\eta_c})} \qquad (3.5)$$

Where p_0=1013mbar, λ=810nm, w_0 is the *beam waist*, η is ionization rate and η_c is critical ionization rate. $\Delta\delta$ is the difference of refractive indexes between each harmonic and the fundamental laser. Consequently, as bigger the ionization rate is, so bigger the pressure of phase matching has to be. When the ionization rate reaches the value η_c, then the achievement of phase matching is not feasible.

Nitrogen is ionized more easily than the other gases. It has higher ionization rate. According to Eq.3.5 we expect Nitrogen for the same intensities of the beam of 810 nm, to present perfect phase matching for higher pressures than the corresponding pressure for the gases Neon and Argon. Pressure p=50 Torr, in which we received spectrum for the three gases (Fig.3.4-3.6) is not the pressure of perfect phase matching for Nitrogen. This ascertainment possibly explains the high difference in harmonic amplitude for Argon, in relation to the other two gases.

3.4 PRESENTATION OF SPECTRA FOR ARGON AT CONSTANT FOCUS POSITION AND VARIABLE PRESSURE.

In the figures below, (Fig.3.10-3.14) the variation of harmonic amplitude is presented as a function of wavelength, for constant focus position and variable pressure of Argon in the cell. We consider that focus position is constant at 3mm before the exit of the cell (z_f=+3mm). The pressure of the Argon fluctuates between 20-60 Torr.

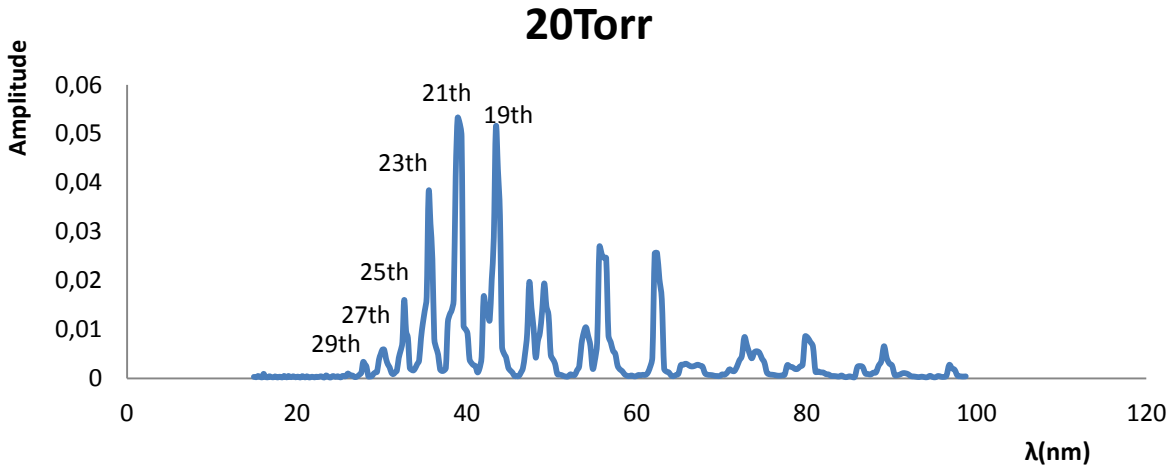

Fig.3.10 *Amplitude of XUV radiation for Argon at pressure p=20 Torr and focus position z_f=+3mm.*

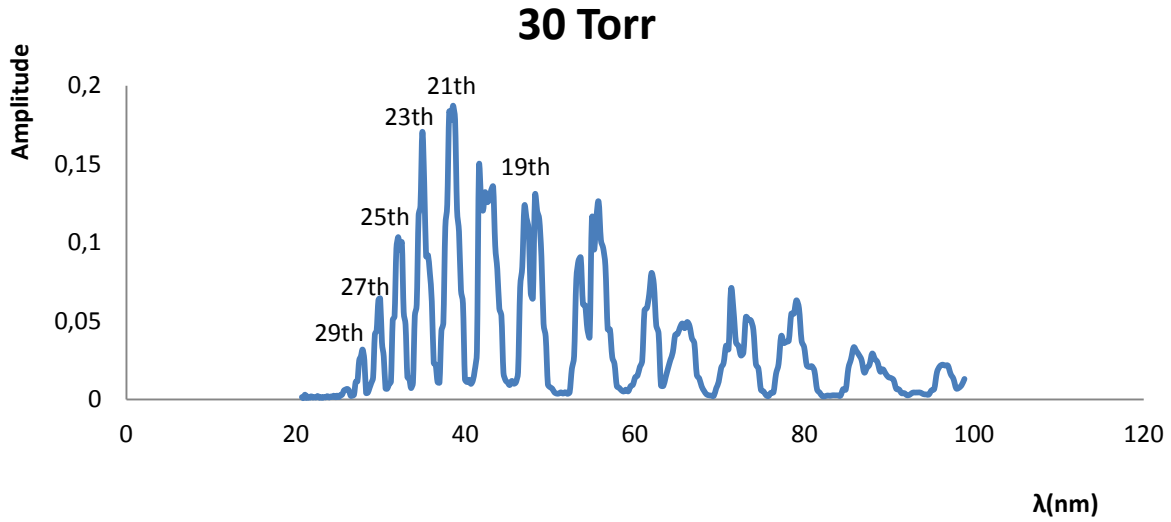

Fig.3.11 *Amplitude of XUV radiation for Argon at pressure p=30 Torr and focus position z_f=+3mm.*

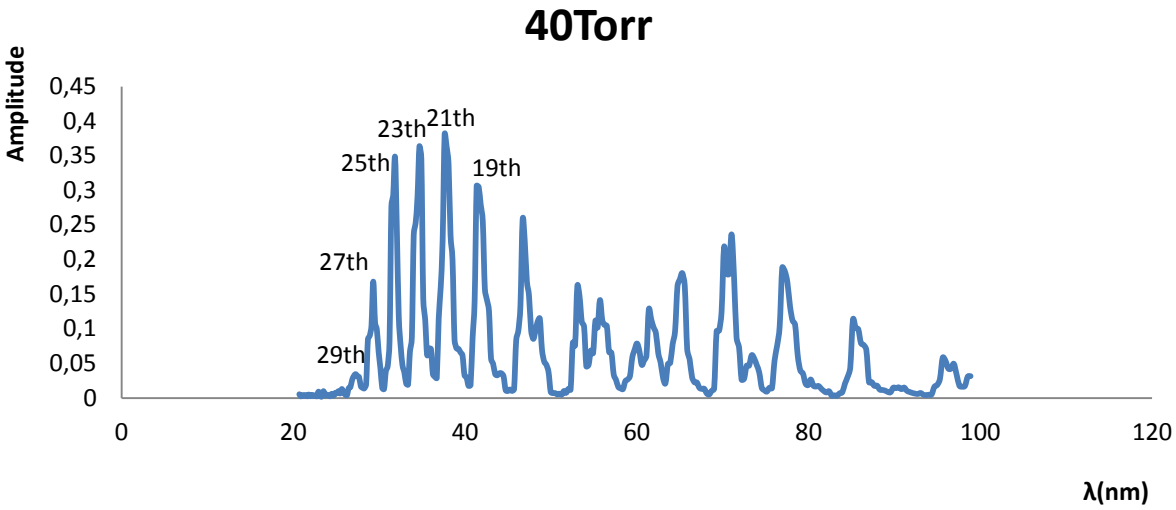

Fig.3.12 *Amplitude of XUV radiation for Argon at pressure p=40 Torr and focus position z_f=+3mm.*

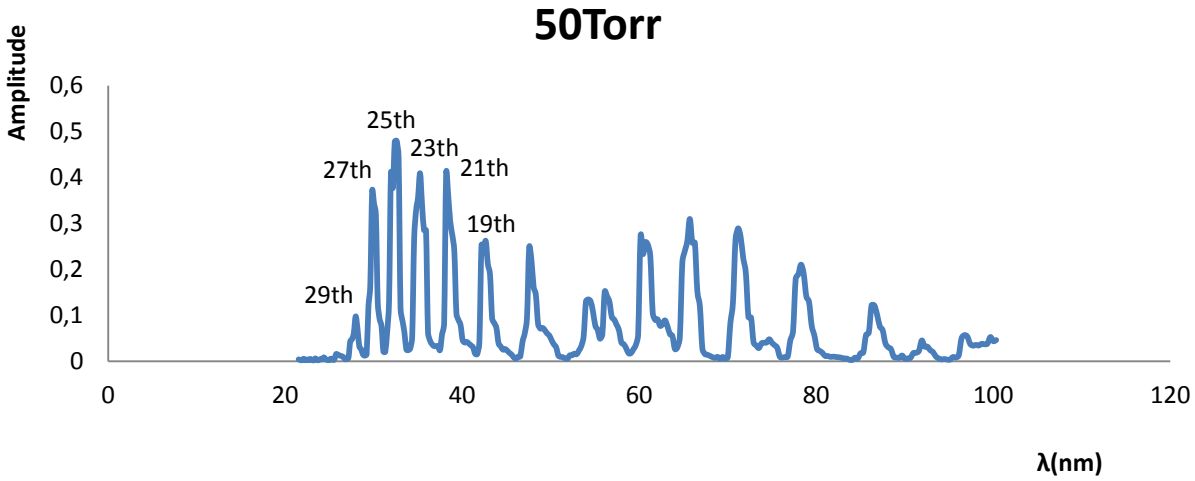

Fig.3.13 *Amplitude of XUV radiation for Argon at pressure p=50 Torr and focus position z_f=+3mm.*

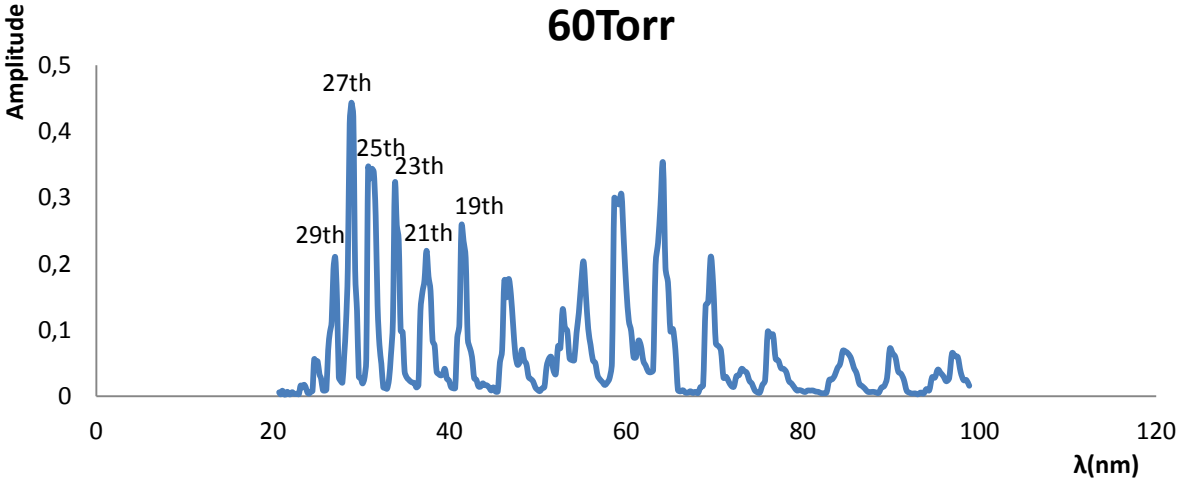

Fig.3.14 *Amplitude of XUV radiation for Argon at pressure p=60 Torr and focus position z_f=+3mm.*

In the following table, the values of amplitude of harmonics 19-29 for pressures 20-60 Torr, are presented.

Harmonic order	Amp.(20 Torr)	Amp.(30 Torr)	Amp.(40 Torr)	Amp.(50 Torr)	Amp.(60 Torr)
19^{th}	0.051	0.132	0.307	0.262	0.257
21^{th}	0.053	0.187	0.380	0.409	0.219
23^{th}	0.038	0.170	0.363	0.409	0.319
25^{th}	0.016	0.103	0.348	0.480	0.343
27^{th}	0.006	0.06	0.168	0.371	0.443
29^{th}	0.003	0.03	0.034	0.100	0.209

Tab.3.5 Amplitude of harmonics 19-29 for pressures 20-60 Torr.

In the following figures (Fig.3.15-3.20), the variation of amplitude for each harmonic (19-29) as a function of the gas pressure in the semi-infinite cell, is presented.

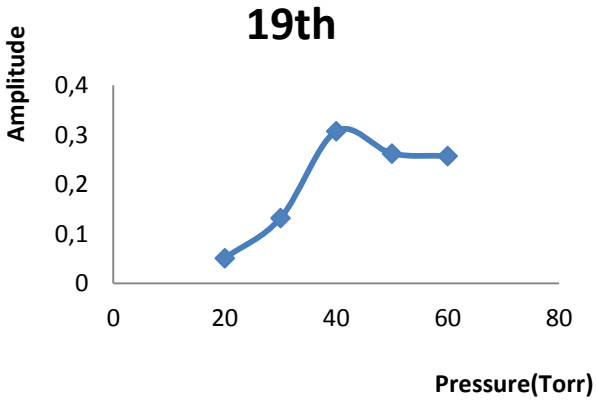

Fig.3.15 Amplitude of 19^{th} harmonic as a function of the pressure of Argon

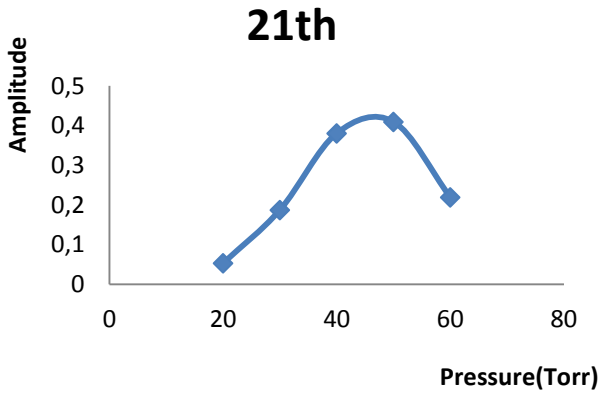

Fig.3.16. Amplitude of 21^{th} harmonic as a function of the pressure of Argon

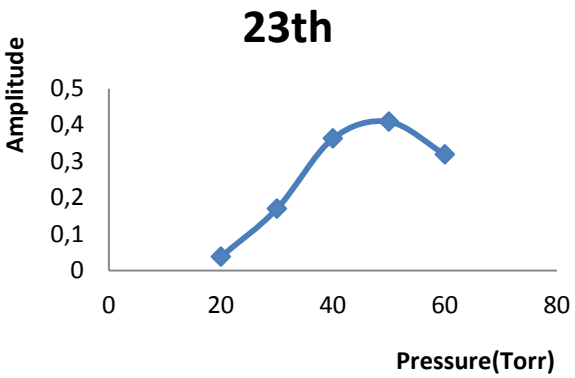

Fig.3.17 Amplitude of 23th harmonic as a function of the pressure of Argon

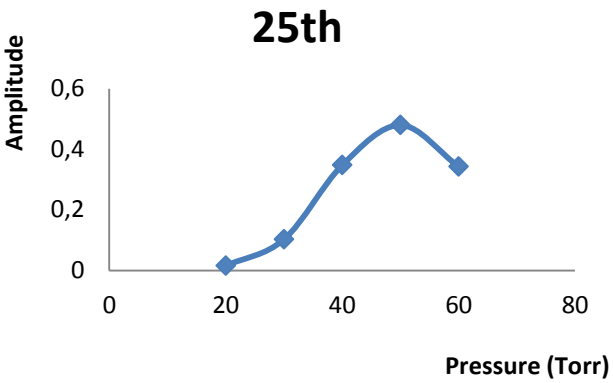

Fig.3.18. Amplitude of 25th harmonic as a function of the pressure of Argon

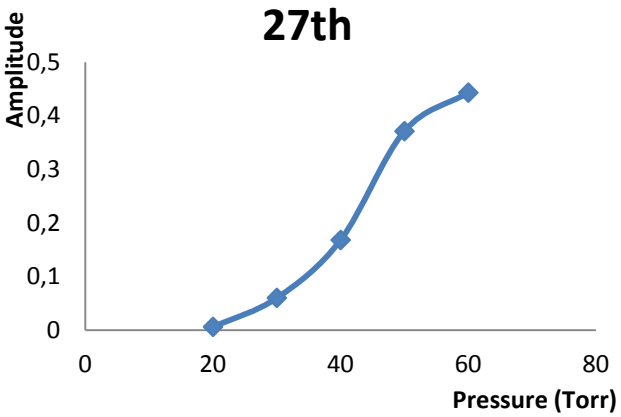

Fig.3.19 Amplitude of 27th harmonic as a function of the pressure of Argon

.

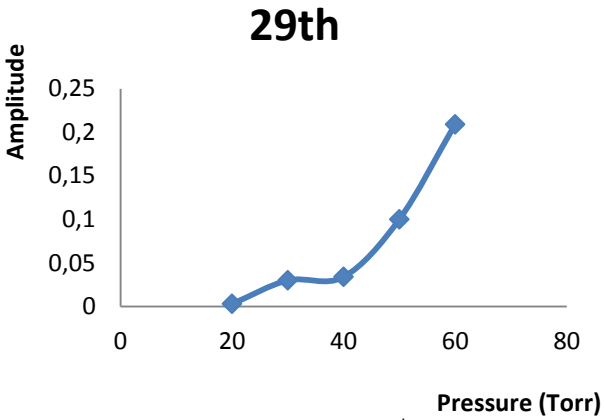

Fig3.20 Amplitude of 29th harmonic as a function of the pressure of Argon

COMMENTS

I) In all of the previous figures we notice that the amplitude of each harmonic generally increases as the pressure increases. This increase is expected as we know that the intensity of each harmonic is analogous to the square of the gas pressure ($I_q \sim p^2$)n we achieve perfect phase matching. However, we notice reduction of intensity of harmonics 19-25 when the pressure becomes higher than 50 Tor. This reduction is observed as the mismatch wave vector between the fundamental laser beam and each harmonic ($\boldsymbol{\Delta\kappa_q}$) depends on the pressure ($\boldsymbol{\Delta\kappa_q = \Delta\kappa_q(p)}$).

The harmonic intensity presents oscillations according to Eq.1.42

$$I_q(P) = \frac{{\omega_q}^2}{n_q(P)(n_0(P))^q c^4 {\varepsilon_0}^2} \left|x^{(3)}(P)\right|^2 {I_1}^q \frac{sin^2\left(\frac{L_q \Delta k_q(P)}{2}\right)}{\left(\frac{L_q \Delta k_q(P)}{2}\right)^2}$$

The number of photons for a harmonic of order q, emmited in the axis, is given, according to [31], by the following equation:

$$N_{out} \propto P^2 {A_q}^2 \frac{4{L_{abs}}^2}{1+4\pi^2 \left(\frac{{L_{abs}}^2}{{L_{coh}}^2}\right)} \left[1 + exp\left(\frac{-L_{med}}{-L_{abs}}\right) - 2cos\left(\pi \frac{L_{med}}{L_{coh}}\right) * exp\left(-\frac{L_{med}}{2L_{abs}}\right)\right] \quad (3.6)$$

$\boldsymbol{P}$ is the gas pressure, $\boldsymbol{A_q}$ is *atomic dipole amplitude*, $\boldsymbol{L_{med}}$ the length of the medium, $\boldsymbol{L_{abs}}$ the length of absorption and $\boldsymbol{L_{coh}}$ the coherence length.

The conditions for optimum phase matching in a gas which presents absorption are:

$$\boldsymbol{L_{med} > 3L_{abs}} \ \& \ \boldsymbol{L_{coh} > 5L_{abs}} \text{ [31]}$$

The coherence length is given by the formula $L_{coh}=\pi/\Delta\kappa$. Consequently, it depends on the gas pressure. The coherence length is maximised when the pressure takes a specific value – ***optimum pressure*** ($\boldsymbol{P_{opt}}$).

The gas pressure affects also the absorption length ($\boldsymbol{L_{abs}}$) for a harmonic. Furthermore these two lengths depend on the order of each harmonic.

From Fig.3.15-3.20 (amplitude-pressure for each harmonic) we conclude that for low pressures, the mismatch wave vector takes higher values. By increasing the pressure, the vector decreases and when the harmonic amplitude maximizes, it takes the value $\Delta\kappa_q=0$ ($L_{coh}\rightarrow\infty$). When the pressure overcomes P_{opt}, the mismatch wave vector increases leading to a reduction of harmonic amplitude.

As mentioned in chapter 1.3, the mismatch wave vector due to dispersion because of plasma generation, is given by Eq.1.35:

$$\Delta\kappa_{qplasma} = \frac{\omega_p(1-q^{2)}}{2qc\omega}$$

We know that $\omega_p \sim \sqrt{N_e}$ and $N_e \sim p$. Consequently an increase of pressure over a specific value, can lead to increase of the term $\Delta\kappa_{q,\ plasma}$ and correspondingly, to reduction of coherence length L_{coh} and of the amplitude of the harmonics which fall onto the *MCP* detector.

Another one possible explanation, in relation to reduction of intensity of generated harmonics, as the gas pressure increases, over a specific value (~50Torr), could be connected with the dependence of focus position by the gas pressure. Specifically, the increase of pressure, is possible to result in focusing closer to cell exit (in front of desireable focus position, q.v. **3.6.2**). In other words, the increase of Argon pressure in the cell, leads to focusing, closer to vacuum chamber, where the detection of harmonics takes place. According to [21] we know that the harmonics are generated more efficiently, when the focusing of the laser beam occurs inside the semi-infinite cell. On the contrary, focusing back of the pinhole could lead to reduction of efficiency of generated harmonics. In Fig. 3.21, the variation of focusing position of the fundamental beam, as the Argon pressure in the cell increases,is shown. The laser beam enters the cell in order to interact with the Argon atoms (From the left part of the figures).

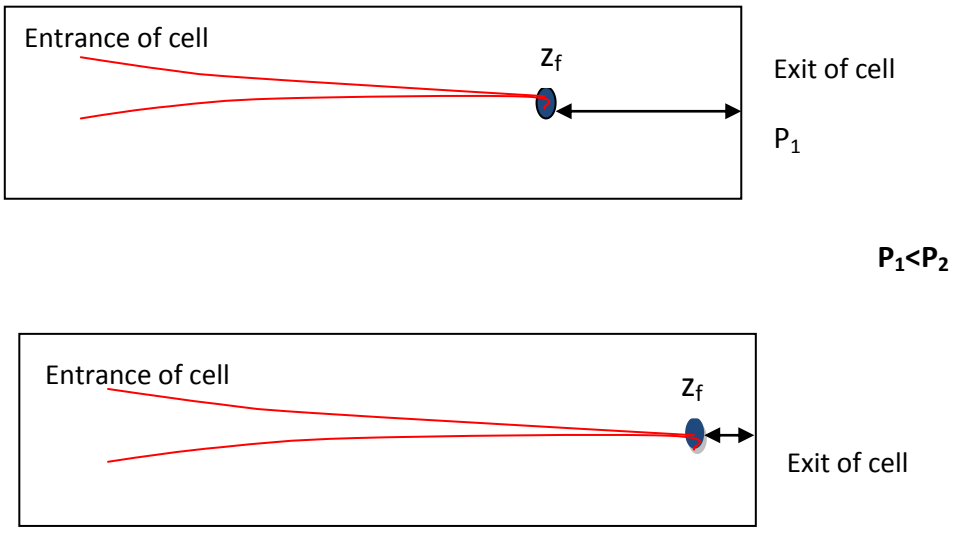

Fig.3.21 Variation of focus position of laser beam, as the Argon pressure in the cell increases.

II) For harmonics 19-25, the pressure in which the maximum of amplitude is recorded, is about p=50Torr. At this pressure, the intensity of the harmonics is maximized.

III) For harmonics of order 27 & 29, the pressure in which the amplitude is maximized, is about 60 Torr. Consequently, as the order of harmonic increases, (from 25 to 29), the pressure of maximum intensity increase too. This experimental result comes to agreement with the experimental finding of *Constant et.al***.**[31]. According to that finding, in Argon, the pressure in which the maximum intensity is observed, (***optimum pressure***), increases with the order of harmonic.

TRASMISSION OF RADIATION AS A FUNCTION OF ARGON PRESSURE-CONNECTION WITH SPECTRA

The calculation of transmission (*T*) as a function of wavelength of radiation for Argon is achieved through the application which is available in the website *https://henke.lbl.gov/*. We consider that the distance which the radiation traverses, from the point of its generation up to the point of its entrance in the high vacuum chamber (where it is detected) is of the order of 3mm. The temperature is constant at 295K (room temperature) and the pressure varies from 20-60 Torr.

In Fig.3.22-3.26 the variation of transmission of radiation, as the Argon pressure varies from 20 – 60 Torr, is presented.

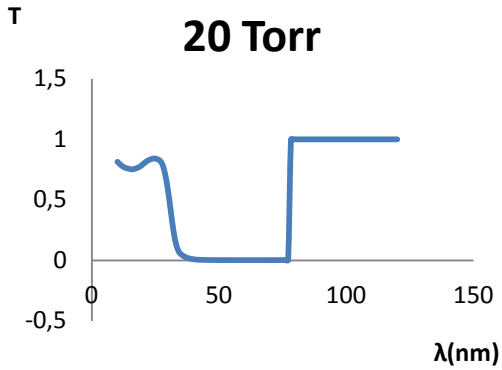

Fig.3.22 Transmission of radiation for Argon as a function of wavelength in nm at p=20Torr.

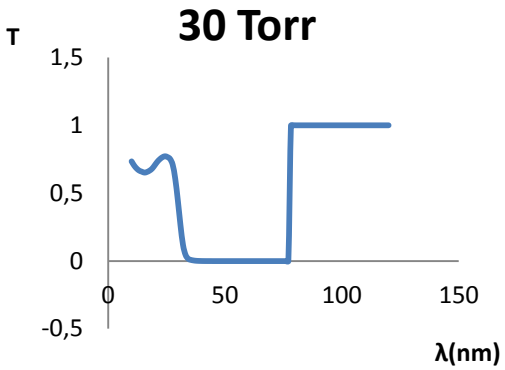

Fig.3.23 Transmission of radiation for Argon as a function of wavelength in nm at p=30Torr.

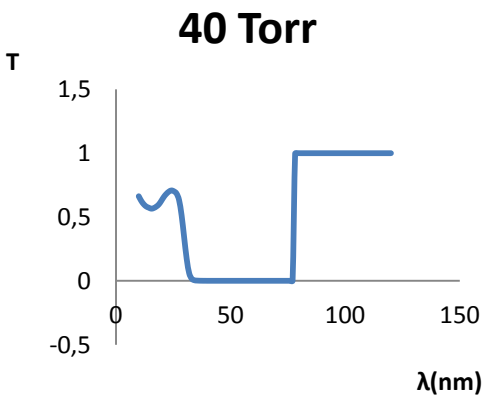

Fig.3.24 Transmission of radiation for Argon as a function of wavelength in nm at p=40Torr.

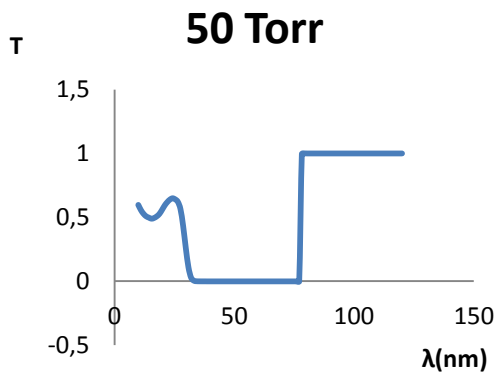

Fig.3.25 Transmission of radiation for Argon as a function of wavelength in nm at p=50Torr.

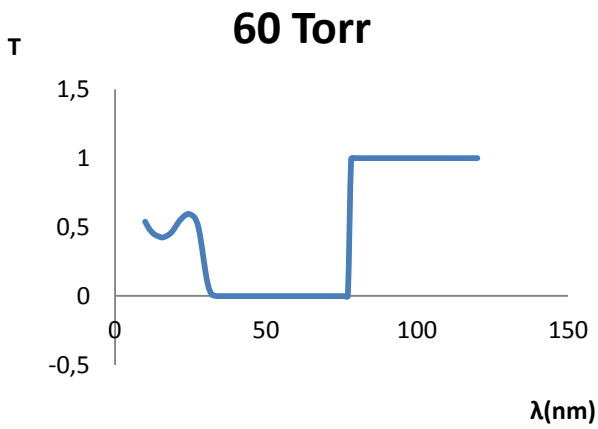

Fig.3.26 Transmission of radiation for Argon as a function of wavelength in nm at p=60Torr.

From the diagrams above, we conclude that the transmission of various wavelengths does not appear important variations, as the pressure increases form 20 to 60 Torr. In all the diagrams, the graphic of transmission as a function of wavelength has the following shape. Firstly for lower wavelengths (10-25nm) the transmission is constant at 0.5. For wavelength λ=25nm the transmission starts to reduce and becomes zero about for λ=30nm. Afterwards, it takes the value 0 for wavelengths 30-75nm. An increase of its value follows and for λ=80nm it takes the value 1 again. We conclude that the transmission takes higher values in the regime of 20-30nm and becomes 0 for λ=50-75nm. The shape of the diagram of the transmission agrees with the behavior of the harmonic spectra (The harmonics in the right part of the spectra – for wavelengths higher than 60 nm- are the the second order of diffraction of the harmonics of the left part of the spectra).

3.5 PRESENTATION OF SPECTRA FOR ARGON AT CONSTANT PRESSURE AND VARIABLE FOCUS POSITION.

In the figures below (Fig.3.27-3.33), the variation of the harmonic amplitude, as a function of wavelength of radiation, is presented for different focus positions of the fundamental beam in the gas cell. The pressure in which we receive the spectra, is constant at p=60 Torr. The focus position can take the values z_f=0-6mm

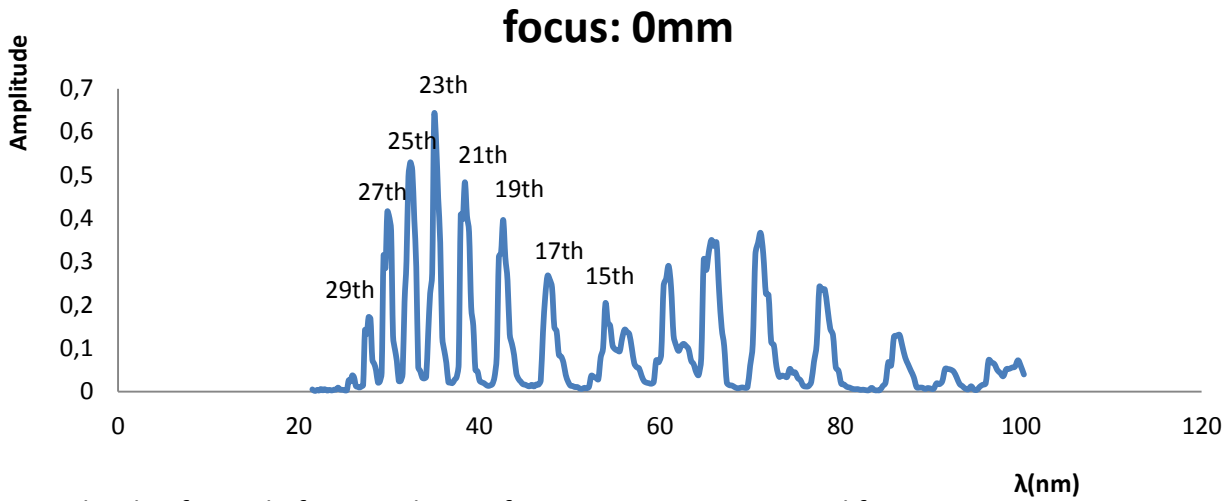

Fig.3.27 Amplitude of signal of XUV radiation for Argon at p=60 Torr and focus position z_f=0mm.

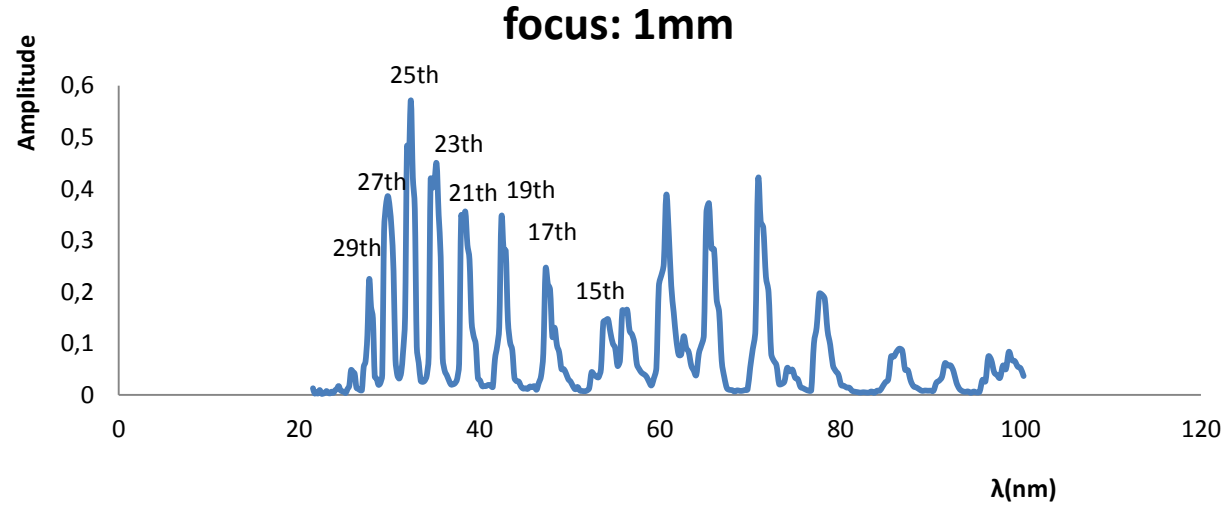

Fig.3.28 Amplitude of signal of XUV radiation for Argon at p=60 Torr and focus position z_f=1mm.

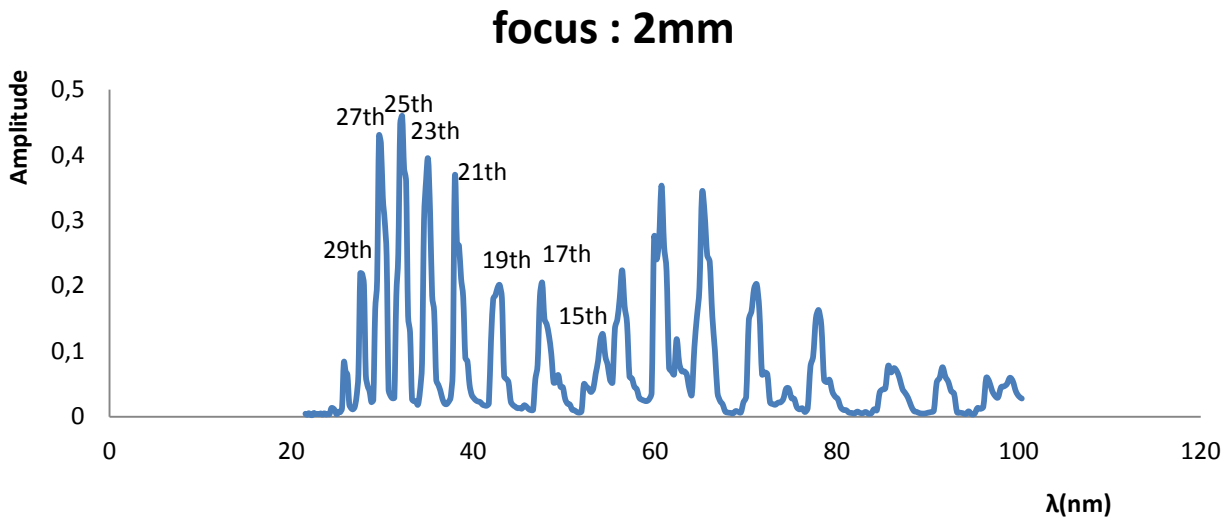

Fig.3.29 Amplitude of signal of XUV radiation for Argon at p=60 Torr and focus position z_f=2mm.

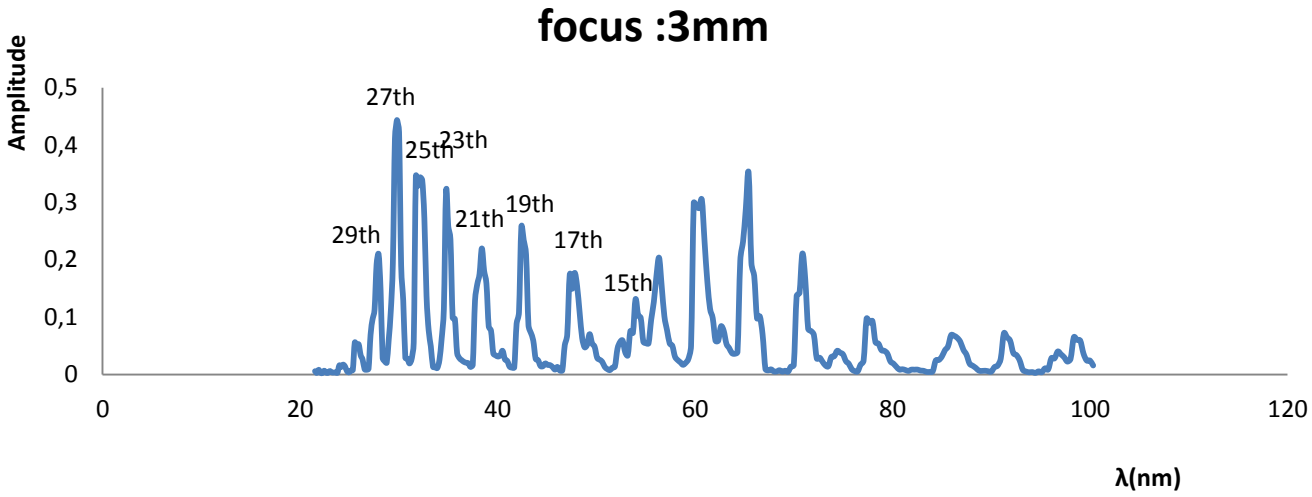

Fig.3.30 Amplitude of signal of XUV radiation for Argon at p=60 Torr and focus position z_f=3mm.

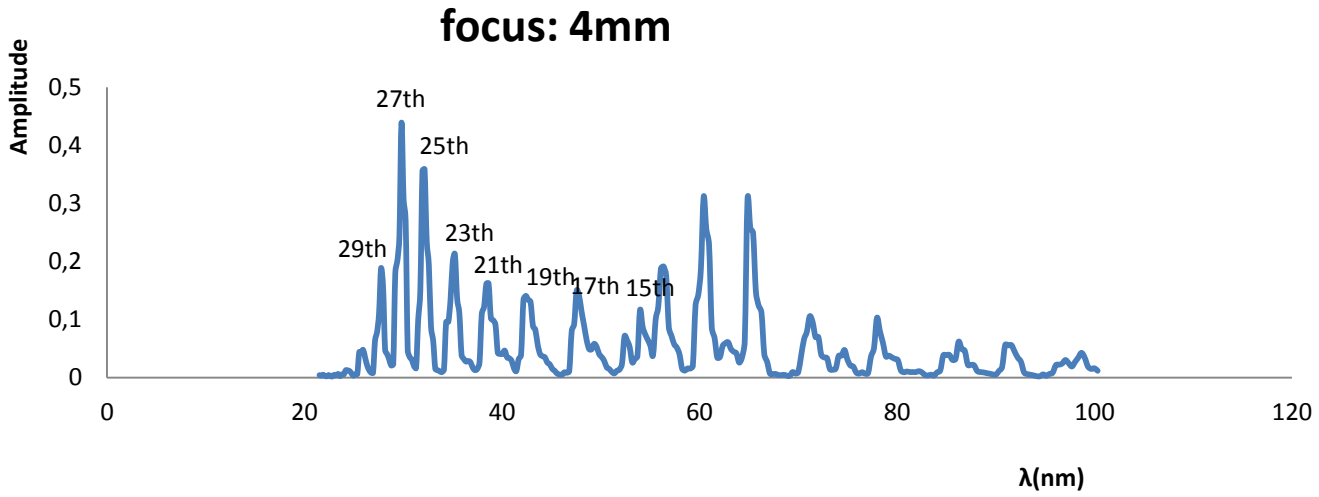

Fig.3.31 Amplitude of signal of XUV radiation for Argon at p=60 Torr and focus position z_f=4mm.

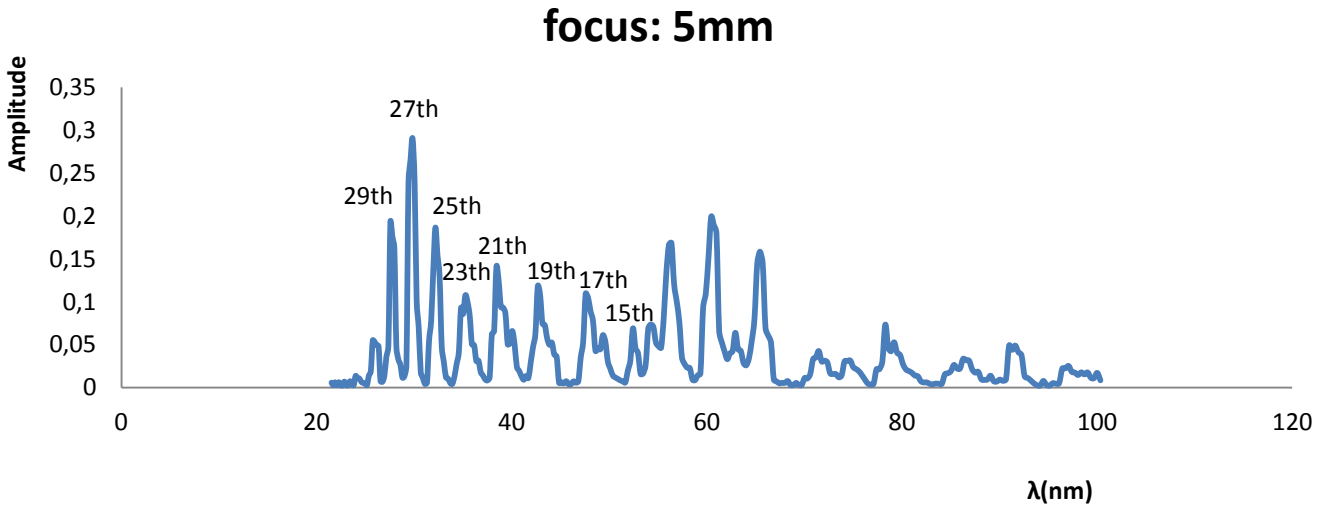

Fig.3.32 Amplitude of signal of XUV radiation for Argon at p=60 Torr and focus position z_f=5mm.

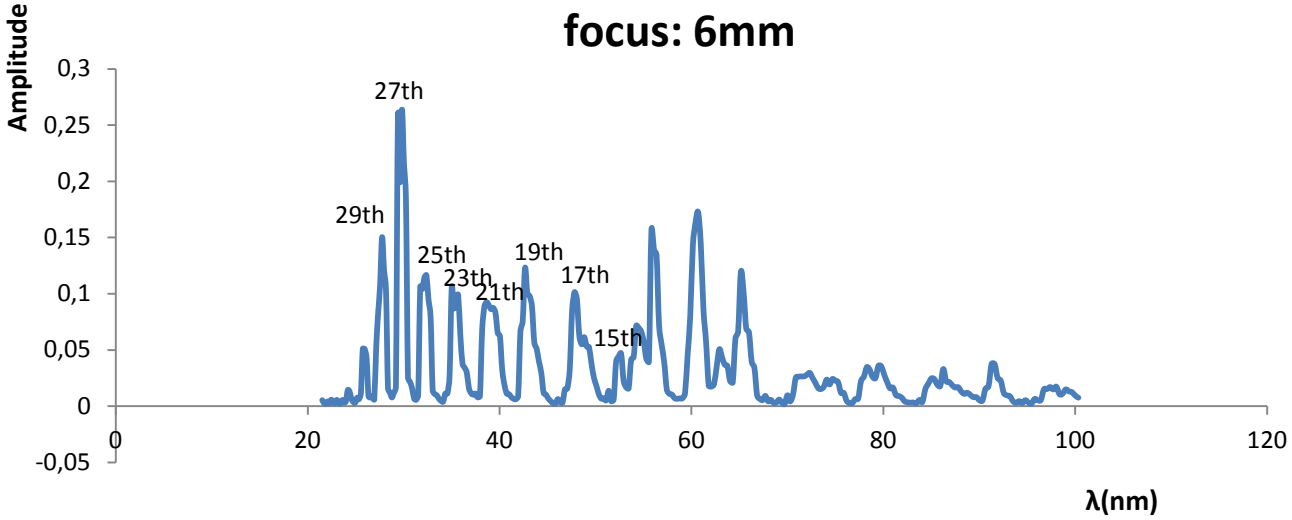

Fig.3.33 Amplitude of signal of XUV radiation for Argon at p=60 Torr and focus position z_f=6mm.

In the following table, the amplitudes of each harmonic (19^{th} -29^{th}) for various focus positions (z_f =0-6mm), are presented.

Harmonic order	**Ampl.** (z_f **=0 mm)**	**Ampl.** z_f **=1mm**	**Ampl.** z_f**=2mm**	**Ampl.** z_f **=3mm**	**Ampl.** z_f **=4mm**	**Ampl.** z_f **=5mm**	**Ampl.** z_f **=6mm**
19^{th}	0.397	0.343	0.200	0.257	0.134	0.117	0.076
21^{th}	0.484	0.355	0.365	0.220	0.161	0.140	0.067
23^{th}	0.637	0.448	O.393	0.319	0.212	0.107	0.105
25^{th}	0.530	0.571	0.447	0.346	0.359	0.186	0.116
27^{th}	0.416	0.386	0.429	0.443	0.438	0.290	0.264
29^{th}	0.173	0.224	0.219	0.210	0.188	0.193	0.150

Tab.3.6 Harmonic amplitudes of orders 19-29 for focus positions z_f= 0-6mm.

We know that the focus position z_f =+3mm corresponds to the spot we expect the beam to be focused on the copper filament. The real position, on which the beam is focused, depends on various factors, which are examined below.

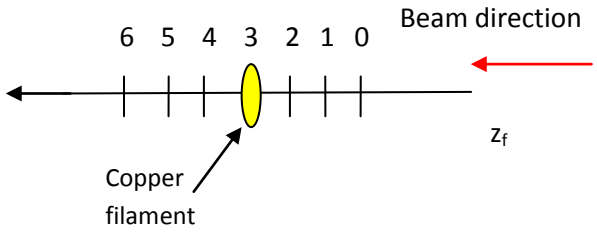

Fig.3.34 Different focus positions of the beam in the semi-infinite cell.

In the figures below (Fig.3.35-3.40), the variation of the amplitude of the harmonics 19-29, for different focus positions (0-6mm), is presented.

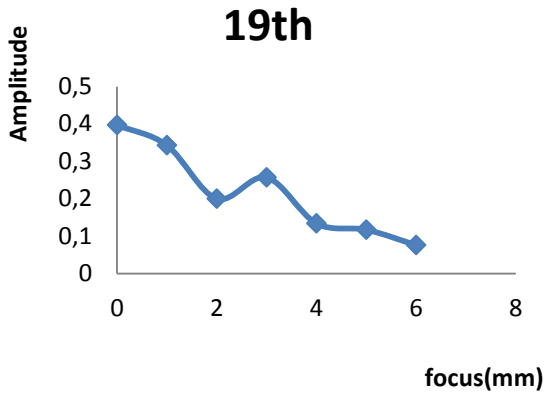

Fig.3.35 Amplitude of 19th harmonic as a function of focus position in the semi-infinite cell.

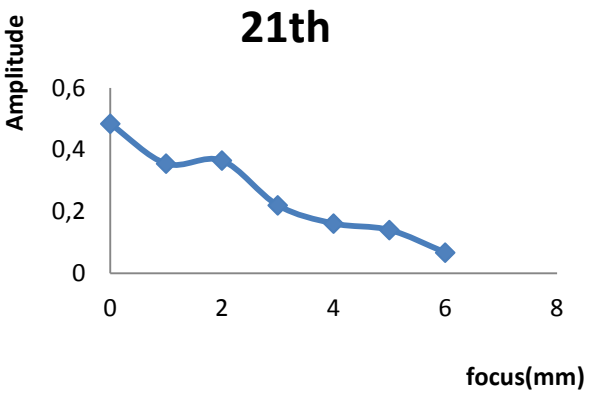

Fig.3.36 Amplitude of 21th harmonic as a function of focus position in the semi-infinite cell.

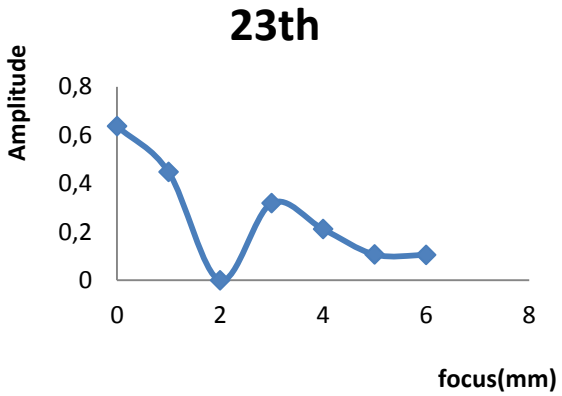

Fig.3.37 Amplitude of 23th harmonic as a function of focus position in the semi-infinite cell.

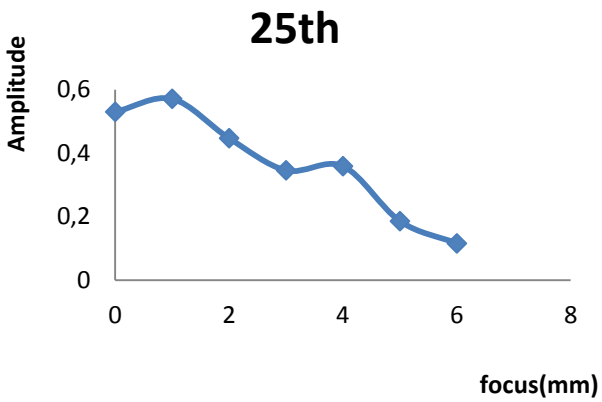

Fig.3.38 Amplitude of 25th harmonic as a function of focus position in the semi-infinite cell.

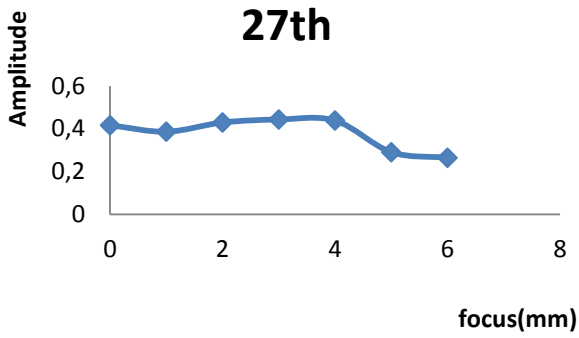

Fig.3.39 Amplitude of 27th harmonic as a function of focus position in the semi-infinite cell.

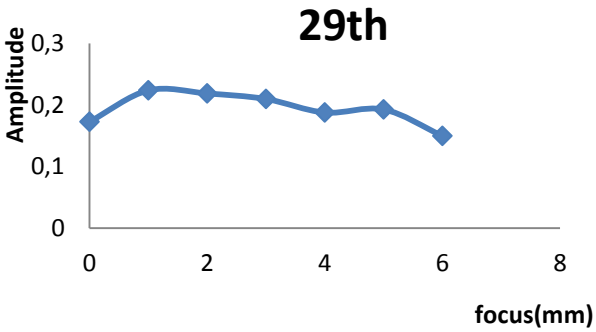

Fig.3.40 Amplitude of 29th harmonic as a function of focus position in the semi-infinite cell.

COMMENTS

I) In Tab. 3.6, the amplitudes of the harmonics, falling on the MCP detector, are recorded. The Tab3.6 lets us to understand the way, which the amplitude of each harmonic varies, separately as the focus position of the beam in the cell takes values z_f =0-6mm. Specifically:

- For the 19th harmonic the amplitude is reduced for z_f=0-2mm. I t displays a low increase for z_f=2-3mm and afterwards it is reduced for z_f=3-6mm.
- For 21th harmonic the amplitude is reduced for z_f=0-1mm. It increases for z_f=1-2mm and afterwards, it is reduced for z_f=2-6mm.
- For 23th harmonic the amplitude is reduced for z_f=0-2mm. It practically takes the value zero. Later it increases for z_f=2-3mm and is reduced for z_f=3-6mm.
- For 25th harmonic the amplitude increases for z_f=0-1mm and is reduced for z_f=1-3mm. It displays a small increase for z_f=3-4mm and is reduced for z_f=4-6mm.
- The amplitude of the 27th harmonic is almost constant for z_f=0-4mm and is reduced for z_f=4-6mm.
- The amplitude of the 29th harmonic doesn't display important variations as the focus position in the semi-infinite cell varies.

II) For all the harmonics we motice that the maximum of their amplitude is observed for **z_f=0mm** or **z_f=1mm**. With other words, the maximum is observed for focus positions at the exit or slightly inside the semi-infinite cell.

The minimum of the amplitude is observed for z_f=6mm for all harmonic orders. An exception is the 23th harmonic, as its amplitude becomes zero for z_f=2mm.

CONNECTION OF AMPLITUDE VARIATION WITH PHASE MATCHING

The minimum of the amplitude is observed for focus positions z_f, in which the geometric term $\Delta\kappa_{q,\,geo}$ due to Gouy phase effect, contributes in the total mismatch wave vector between each harmonic and the fundamental laser beam. For positions in which the amplitude becomes zero (e.g. for focus position z_f=+2mm, for 23th harmonic), the interference between the fundamental beam and the harmonic is destructive.

Another way to control the contribution of the geometrical term in the mismatch wave vector (phase mismatch), is the displacement of the focus position of the beam, relatively to the medium, where the harmonics are generated. From the diagrams above, we find out that the focusing inside the cell (z_f=0mm or z_f=1mm) favors the increase of the high order harmonics 19-29. The value of the geometric term $\Delta_{\kappa q,\,geo}$ is lower for focus positions inside the semi-infinite cell, comparetively with the corresponding focus positions out of the cell.

Furthermore, the focusing of the beam on different positions in the cell, affects the length of the medium, in which the harmonic generation takes place. As a result it favors or makes difficult the achievement of phase matching.

As we mentioned in previous chapter for perfect phase matching, the following conditions have to be fulfilled $\mathbf{L_{med} > 3L_{abs}}$ **&** $\mathbf{L_{coh} > 5L_{abs}}$, where $\mathbf{L_{med}}$ is the length of the medium, $\mathbf{L_{abs}}$ is the absorption length of each harmonic and $\mathbf{L_{coh}}$ is the coherence length.

We consider that the length of the medium is the area in which the interaction between the fundamental laser beam and the atoms of the gas in the cell takes place. With other words, it is the area, in which due to partial ionization, plasma is generated in subsequent time (order of ns up to μs). The plasma illuminates

mainly, because of the recombination of electrons with the nuclei. As we can see from Fig 3.21 this length varies in relation to the focus position of the beam of 810 nm, we use for harmonic generation.

The further from the cell exit the focusing takes place, the bigger the quantity $\mathbf{L_{med}}$ is. On the contrary, focusing near the exit of the cell reduces the length of the medium.

The absorption length $\mathbf{L_{abs}}$ is different for each harmonic of order q. For this length the harmonic intensity has decreased at 1/e of its maximum value.

Finally, the coherence length is the length that the phase difference between each harmonic and the fundamental beam is smaller than π and constructive interference takes place.

The coherence length is given by Eq.1.21:

$$L_{coh}=\frac{\pi}{\Delta\kappa_q}$$

The quantity $\Delta\kappa_q$ is the sum of four different terms according to Eq.1.24:

$$\Delta\kappa_q=\Delta\kappa_{q,geo}+\Delta\kappa_{q,plasma}+\Delta\kappa_{q,neutral}-\Delta\kappa_{q,dip}$$

From Eq.1.28:

$$\Delta\kappa_{q,geo}=\frac{q-1}{z_R\left[1+\left(\frac{z}{z_R}\right)^2\right]}$$

we conclude that the geometric term of phase mismatch wave vector depends on the focus position z_f. As the focus position changes, the quantity $\Delta\kappa_{q,geo}$ varies too and consequently the whole vector $\Delta\kappa_q$. In a similar way, as the focus position changes, the coherence length takes a different value each time.

To sum up, the focusing of the beam on different positions in the semi – infinite cell, is responsible for the variation of such the medium length in which the interaction takes place, as of the the coherence length between the beam of 810 nm and each harmonic.

In Fig 3.35-3.40, the maximum values of the amplitude of each harmonic, are observed when the phase matching conditions are optimally fulfilled and the vector $\Delta\kappa_q$ has the lowest value.

Finally, from Eq.1.28 we notice that the phase mismatch wave vector $\Delta\kappa_{q,geo}$ is analogous to *q-1*, for specific focus positions of the laser beam. With other words, it takes higher values for harmonics of higher order. Consequently the total mismatch wave vector increase too (The contribution of the $\Delta\kappa_{q,geo}$ term is positive -$\Delta\kappa_{q,geo}$>0). Increase of the total wave vector results in reduction of the coherence length $\mathbf{L_{coh}}$.

From Fig.3.39-3.40 we notice that the maximum value of the amplitude of the harmonics of order 27 & 29 is lower in relation to the corresponding maximum values of the harmonics of order 19& 25 (Fig.3.35 - 3.38). This difference is possibly connected with the fact that for the same focus position, the harmonics of higher order *q*, display bigger phase mismatch $\Delta\kappa_q$ with the fundamental beam.

3.6 FOCUS POSITION OF THE FUNDAMENTAL BEAM IN THE SEMI-INFINITE CELL

As mentioned in chapter 2.4, the fundamental laser beam can be focused through a mirror of focal distance f=30cm, on different positions in the semi-infinite gas cell. However, the position in which the interaction, betwwen the laser beam and the atoms of the gas happens, is not always the same with the position we expect the beam to be focused by removing the lens. We expect the position in which the beam focuses on the copper filament (at the exit–pinhole of the cell), to be for z_f =+3mm. By increasing z_f, the expected focus position is replaced out of the cell. Correspondingly, by reducing z_f, we expect the focus position to move towards the interior of the semi-infinite cell.

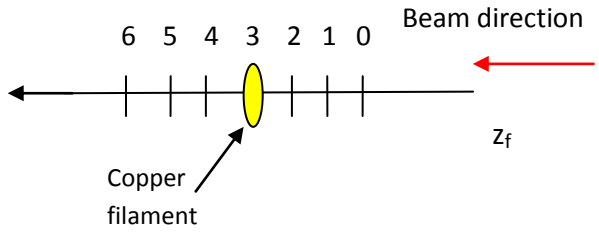

Fig 3.41 Schematic layout of the positions we expect the beam to be focused in relation to the exit of the cell, by removing the focusing lens. For position z_f =+3mm, we consider that the interaction takes place on the copper filament, at the exit of the cell.

Some factors which determine the focus position of the beam and its interaction with the atoms of the gas are the following:

1)The position that the lens is put in front of semi-infinite cell.
2)The pressure of the gas in the cell.
3)The dynamic balance between nonlinear focusing of the beam due to Kerr effect and its defocusing by the generated plasma (plasma defocusing)

Later, we make an attempt to investigate the way that the factors above, are related to the focus position of the laser beam in the semi-infinite cell.

I) REMOVAL OF THE POSITION OF THE FOCUSING MIRROR

As we mentioned in chapter 2.4 of the master thesis, the focusing lens of the fundamental beam, can be removed by a micro-scale system of Verner type. By rotating the mechanism in which the lens is located, we can change the position in which it focuses the beam. Two rotations of the impeller correspond to displacement of the lens by 1mm.

II) CONNECTION OF THE FOCUS POSITION WITH THE GAS PRESSURE IN SEMI-INFINITE CELL.

The pressure of the gas in semi-infinite cell (specifically for Argon) is a factor which affects the real focus position of the beam, to achieve interaction with the atoms of the medium.

The pressure of Argon in semi-infinite cell is variable. It fluctuates between 20-60 Torr. By increasing the pressure of Argon, the number of electrons per volume unit (N_e) increases too.

According to Eq.1.33 ($n_p = 1 - \frac{1}{2}(\frac{\omega_p}{\omega})^2)$ the refractive index of the medium is reduced as the contribution of the plasma becomes intense. The generated plasma can act as a defocusing mirror, resulting in the focusing of the laser beam towards the exit of the cell. With other words, the focus position can be shifted in front of the position we desire to focus the beam with the lens (As the laser beam enters the semi-infinite cell).

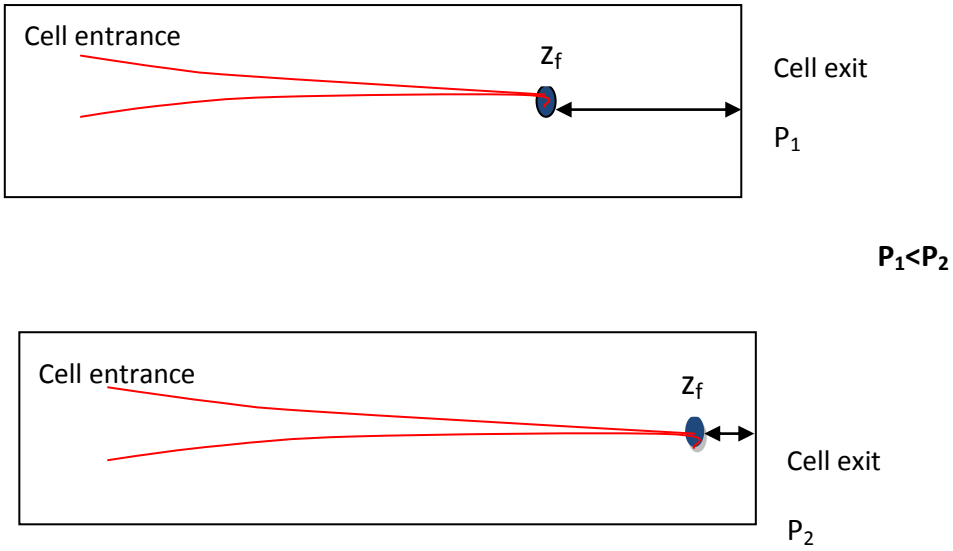

Fig.3.42 Displacement of the focus position of the beam, because of the variation of gas pressure in the cell. The desireable focus position can be removed towards the exit of the cell due to the increase of Argon pressure.

III) DYNAMIC BALANCE BETWEEN NONLINEAR FOCUSING OF THE BEAM DUE TO *KERR EFFECT* AND DEFOCUSING BY THE GENERATED PLASMA (*PLASMA DEFOCUSING*).

The focus position of the fundamental laser beam in the cell, in order to interact with the atoms of Argon and generate harmonics, is not always the same with the expected position. Two factors, which are antagonistic, affect the focus position of the beam. These factors are: the self focusing of the beam because of Kerr effect and the defocusing due to the generated plasma (plasma defocusing).

According to Kerr effect, the refractive index of a non-linear medium increases when an electric field of high intensity I, is applied. The refractive index is given by the formula:

$$n=n_0+n_2 I$$

n_0 is the weak field refractive index and n_2 is a term which refers to the rate that the refractive index increases with the intensity of the beam.

Consequently, when a laser beam of high intensity travels in a nonlinear medium, increase of its refractive index is caused. The medium becomes denser, resulting in self focusing of the beam.

In opposition to Kerr effect, the generation of plasma functions. When a laser beam travels in a medium, its atoms are ionized and plasma is generated.

According to Eq.1.31 the induced refractive index due to the existence of plasma is:

$$n_p = \sqrt{1-\frac{{\omega_p}^2}{\omega^2}} = \sqrt{1-\frac{N_e}{N_c}}$$

We notice that plasma generation causes reduction of the refractive index of the medium. With other words, the plasma acts as defocusing mirror. The defocusing of the beam, due to plasma, is possible to result in different focus positions from those we would like to achieve by removing the lens which focuses the beam in the cell.

CHAPTER 4.CONCLUSIONS

In the last chapter of this master thesis, the conclusions coming from analysis of experimental data are presented.

We studied HHG from three different gases. The source of harmonic generation is the pulsed laser Ti-Sa Pulsar, with duration 25fs and Peak Power 45TW. The energy per pulse of the beam, we use for harmonic generation is 1.2 mJ for gases Argon and Neon and 1.08 mJ for Nitrogen.

In the first chapter, the semi-classical model of Three Steps (Three Step Model) is described. It describes the stages of harmonic generation when the laser beam interacts with the atoms of the gas. Furthermore, the factors which determine the phase mismatch between each harmonic and the fundamental beam are investigated.

Later, there is reference to ***Quasi Phase Matching*** technique. At the end, the layout of a semi-infinite cell and the factors which affect HHG are described. We put emphasis on CPA technique, which is used for the amplification of laser pulse. The main parts of experimental set up are also described and analyzed separately.

In the third chapter, the recorded spectra of radiation for the three gases are cited. Firstly, we compare the spectra for the three gases at the same pressure. Furthermore, for gases Argon and Neon, the focus position and the energy of the beam are the same (z_f =*3mm*, energy per pulse: 1.2mJ). For Nitrogen, the energy of the beam is slightly lower (1.08mJ). The focus position in which we record signal for Nitrogen is z_f=8mm.

As regards the differences appearing in the harmonic amplitudes for the three gases, we conclude that they possibly arise due to various factors. The interpretation of these differences is a complicated issue.

In this master thesis we attempted to associate the differences in harmonic amplitude with factors such:

- Radiation absorption as a function of wavelength.
- The different ionization potential of the gases.
- The energy of the fundamental laser beam.
- The focus position of the beam in the cell, in order to interact with the atoms of the gas.

Afterwards, for Argon we cite spectra in the same focus position for five different pressures (20-60Torr). Finally, for constant pressure=50Torr, spectra for different focus positions of the beam, are presented.

In the case of Argon, we conclude that for low pressures (20-50 Torr), the intensity of harmonics varies as $Iq \sim p^2$. By increasing the pressure over a specific value $P_{opt,}$ the intensity decreases. The value of pressure is P_{opt} =50Torr. At this pressure, conditions for perfect phase matching are optimally fulfilled (q.v. Chapter 1.3).

For higher pressures, it is possible the generated plasma to function as a defocusing mirror, resulting in the focusing of the beam in front of the exit of the cell.

Another parameter which affects the amplitude of the detected harmonics is the focus position of the beam into the cell. The focus position can be selected by using a focusing mirror. However, the focus position does not always identify with the expected one.

Some factors which affect the focus position of the beam in the cell are:

- The gas pressure
- The self focusing of the beam due to *Kerr Effect*
- The defocusing of the beam due to the generated plasma

Furthermore, we make an attempt to explain the variations of the amplitude of generated harmonics for Argon, as the focus position varies between z_f*=0-6mm.* It is found that:

- The harmonic amplitude takes its maximum value for focus positions z_f =0-1mm. With other words, the harmonic generation near the exit of the semi-infinite cell, towards its interior, is amplified.
- A way to control the detected harmonic amplitude is the removal of focus position.
- For focus positions z_f =0-1mm, conditions for perfect phase matching are fulfilled between the harmonics and the fundamental beam (**$L_{med} > 3L_{abs}$ & $L_{coh}>5L_{abs}$**).

The experimental results of this master thesis show that the structure of a semi-infinite cell is an ideal medium for HHG in gases. That is why:

- It presents consistency and repeatability.
- It is a compact, table-top structure.
- We come to conclusions by altering each time a parameter and keeping all the other parameters constant.
- The geometry of the experimental set up lets the macroscopic control of parameters and their values at constant level. Such parameters are the gas pressure and the intensity of laser beam. The pressure is controlled by a needle valve, while the intensity of the beam is controlled through CPA technique.

The Semi-Infinite Gas Cell can act as a source of coherent radiation in Soft X-ray radiation and XUV part of the spectrum. This coherent radiation can be useful for various sciences such as:

- Physics
- Chemistry
- Biology
- Biochemistry

Specifically, applications can be found in domains [32-36], unexplored in the past, such as:

- Atomic and Molecular Spectroscopy
- Condensed Matter Physics
- Plasma Physics
- Imaging in nano-scale

The last use of generated radiation in semi-infinite cell is based on the fact that the wavelengths of generated harmonics fluctuate in the area of nanometers. Low wavelength corresponds to high resolution.

The detected harmonics by MCP detector have wavelengths 20-100 nm. Such a radiation in Soft X-ray and XUV part of the beam, which presents high coherence and intensity, can be used for a new technique, known as ***Coherent Diffractive Imaging*** [37].

This technique lets us to overcome the limit of resolution of optical microscopes (200nm). Furthermore, it is better than electron spectroscopy, because the mean free path of charged particles is not appropriate for the imaging of samples with dimensions lower than 500nm. In addition, the thickness of some biological samples doesn't favor the imaging through electron beam [37].

CDI technique:

- Does not require the use of focusing mirror (*lensless technique*).
- Opens new ways in domains such as Biology and Material Science.
- It offers the capability of imaging of nanostructures such nanocrystals, defects, biomaterials, proteins etc.[38]

The way this technique functions is based on the scattering of radiation by the irradiated object and the creation of dark and bright diffraction fringes (diffraction pattern) which are collected by the detector. This coherent XUV radiation irradiates the surface, which is examined at various points, in order to obtain a view of the whole object. Afterwards, through a computing algorithm, the diffraction fringes are turned into an image of the object. This collected image is aberration free.

To sum up:

- The Semi-Infinite Gas Cell can act as a coherent source of radiation in the area of ***Soft X-ray radiation*** and ***XUV*** (ultra violet) part of the spectrum, with numerous applications in unexplored in the past domains.
- The study of the spectrum of high order harmonics in semi-infinite cell is a complicated issue. It is necessary to examine various parameters in order to understand the variations appearing in the spectra recorded by the computing program.
- The way each one from the factors above, affects the spectrum of detected radiation is not determinate.
- By comparing the amplitude differences of each harmonic when the gas pressure or the focus position of the beam in the cell change, we attempt to explain the physical mechanism behind them (phase matching theory, absorption of radiation, variation of focus position, ionization potential of the gas).

BIBLIOGRAPHY

[1] N.Papadogiannis et al., Applied Physics B 73, 687 (2001).

[2]A. Rundquist et al., Science 280, 1412 (1998).

[3] N. A. Papadogiannis, B. Witzel, C. Kalpouzos, and D. Charalambidis, Phys. Rev. Lett. 83, 4289(1999).

[4] K. Kosma, S. A. Trushin, W. Fuss, and W. E. Schmid, The Journal of Physical Chemistry A 112, 7514 (2008)

[5] A.Peralta Conde et al., Phys.Rev.A 79,061405 (2009).

[6] P. B. Corkum, Phys. Rev. Lett. 71, 1994 (1993).

[7] B. K. Dinh, Ph.D. thesis, Swinburne University of Technology Melbourne, 2012.

[8] L. V. Keldysh, "Ionization in the field of a strong electromagnetic wave," *Sov. Phys. JETP 20*, p.1307–1314, 1965.

[9] M. V. Ammosov, N. B. Delone, and V. P. Krainov, "Tunnel ionization of complex atoms and of atomic ions in an alternating electromagnetic field," *Soviet physics JETP*, *64:1191–1194*, 1986

[10] T. Pfeifer, C. Spielmann, and G. Gerber, Reports on Progress in Physics 69, 443 (2006).

[11] A. L. Lytle, “Phase Matching and Coherence of High Order Harmonic Generation in Hollow Waveguides” PhD thesis, University of Colorado (2008)

[12] H. Dachraoui et al., Journal of Physics B: Atomic, Molecular and Optical Physics 42, 175402 (2009)

[13] J.Rothhardt et al., New Journal of Physics 16, 033022 (2014).

[14]W. L. a. A. P. H.J. LEHMEIER, "NONRESONANT THIRD ORDER HYPERPOLARIZABILITY OF RARE GASES AND N 2 DETERMINED BY THIRD HARMONIC GENERATION," *OPTICS COMMUNICATIONS Volume 56, number 1,* 1985

[15] Paul A, Bartels R A, Tobey R, Green H, Weiman S, Christov I P, Murnane M M, Kapteyn H C and Backus S, "Quasi-phase-matched generation of coherent extreme ultraviolet light," *Nature 42 51–4*, 2003.

[16] Zepf M, Dromey B, Landreman M, Foster P and Hooker S M, "Bright quasi-phase-matched soft x-ray harmonic radiation from argon ions," *Phys. Rev. Lett. 99 143901*, 2007

[17] Dromey B, Zepf M, Landreman M and Hooker S M, "Quasi-phase-matching of harmonic generation via multimode beating in waveguides," *Opt. Express 15 7894–900*, 2007

[18]A. Willner, F. Tavella, M. Yeung, T. Dzelzainis, C. Kamperidis, M. Bakarezos, D. Adams, M.Schulz, R. Riedel, M.C. Hoffmann, W. Hu, J. Rossbach, M. Drescher, N.A. Papadogiannis, M.Tatarakis, B. Dromey, and M. Zepf, "Coherent control of high harmonic generation via dual-gas multijet arrays," *Phys. Rev. Lett. 107*, *175002*, 2011

[19] A Willner, F Tavella, M Yeung, T Dzelzainis,C Kamperidis, M Bakarezos, D Adams, R Riede,7, M Schulz, M C Hoffmann, W Hu, J Rossbach, M Drescher, V S Yakovlev, N A Papadogiannis, M.Tatarakis, B. Dromey and M Zepf, "Efficient Control of Quantum Paths via Dual-Gas High Harmonic Generation. New J. Phys. 13, 113001 (2011)," *New J. Phys. 13*, *113001*, 2011

[20]Gaudiosi D M, Reagan B, Popmintchev T, Grisham M, Berrill M, Cohen O, Walker B C, MurnaneM M, Kapteyn H C and Rocca J J, "High-order harmonic generation from ions in a capillary discharge," *Phys. Rev. Lett. 96 203001*, 2006

[21] Daniel S. Steingrube, Tobias Vockerodt, Emilia Schulz, Uwe Morgner, and Milutin Kovačev, ''Phase matching of high-order harmonics in a semi-infinite gas cell'', Phys. Rev. A **80**, 043819 – Published 19 October 2009

[22]D. Strickland and G. Mourou, Opt. Commun. 56, 219 (1985)

[23] https://www.nobelprize.org/prizes/physics/2018/summary/

[24] G. Cheriaux, F.Salin and al.,"Aberration-free stretcher design for ultra-short pulse amplification" OPTICS LETTERS March 15 1996).

[25] Oriel instruments, grating physics page

[26] Hitachi grating manual

[27] Hitachi grating information

[28] Ladislas Wiza, J. (1979). *Microchannel plate detectors. Nuclear Instruments and Methods, 162(1-3), 587–601*

[29] https://www.rp-photonics.com/microchannel_plates.html

[30] Heyl C, Güdde J, L'Huillier A and Höfer U."High-order harmonic generation with μJ laser pulses at high repetition rates'' J. Phys. B: At. Mol. Opt. Phys. 45 074020, 2012

[31] E. Constant, D. Garzella, P. Breger, E. Mével, Ch. Dorrer, C. Le Blanc, F. Salin, and P. Agostini "Optimizing High Harmonic Generation in Absorbing Gases: Model and Experiment "Phys. Rev. Lett. 82, 1668 – Published 22 February 1999

[32] J. Zhou, J. Peatross, M.M. Murnane, H.C. Kapteyn, I.P. Christov, Phys. Rev. Lett. 76 (1996) 752.

[33] J.J. Macklin, J.D. Kmetec, C.L. Gordon, Phys. Rev. Lett. 70 (1993) 766.

[34] P.B. Corkum, N.H. Burnett, M.Y. Ivanov, Opt. Lett. 19 (1994) 1870

[35] I.P. Christov, M.M. Murnane, H.C. Kapteyn, Phys. Rev. Lett. 78 (1997) 1251.

[36] Z. Chang, A. Rundquist, H. Wang, M.M. Murnane, H.C. Kapteyn, Phys. Rev. Lett. 79 (1997) 2967.

[37] R. L. Sandberg, A. Paul, D. A. Raymondson, S. Hädrich, D. M. Gaudiosi, J.Holtsnider, R. I. Tobey, O. Cohen, M. M. Murnane, H. C. Kapteyn, C. Song, J.Miao, Y. Liu, and F. Salmassi, "Lensless diffractive imaging using tabletop coherent high-harmonic soft x-ray beams," Physical Review Letters 99, 098103 (2007).

[38] Jianwei Miao, Richard L. Sandberg, and Changyong Song, “Coherent X-ray Diffraction Imaging” IEEE Journal of Selected Topics in Quantum Electronics (Volume: 18, Issue: 1 , Jan.-Feb. 2012)